Marine Geology 463 (2023) 107121

Contents lists available at ScienceDirect

Marine Geology

journal homepage: www.elsevier.com/locate/margo

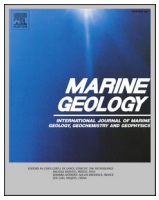

Rising snow line: Ocean acidification and the submergence of seafloor geomorphic features beneath a rising carbonate compensation depth

Peter T. Harris [a,*], Levi Westerveld [a], Qianshuo Zhao [b], Mark John Costello [c]

[a] GRID-Arendal, P.O. Box 183, N-4802 Arendal, Norway
[b] Ocean University of China, Qingdao, People's Republic of China
[c] Nord University, Universitetsalléen 11, 8026 Bodø, Norway

ARTICLE INFO

Editor: Michele Rebesco

Keywords:
Carbonate compensation depth
Ocean acidification
Seafloor geomorphology
Calcareous sediment
Climate change

ABSTRACT

Due to burning of fossil fuels, carbon dioxide is being absorbed by the ocean where its chemical conversion to carbonic acid has already caused the surface ocean to become more acidic than it has been for at least the last 2 million years. Global ocean modeling suggests that the carbonate compensation depth (CCD) has already risen by nearly 100 m on average since pre-industrial times and will likely rise further by several hundred meters more this century. Potentially millions of square kilometres of ocean floor will undergo a rapid transition in terms of the overlying water chemistry whereby calcareous sediment will become unstable causing the carbonate "snow line" to rise.

We carried out a spatial analysis of seafloor geomorphology to assess the area newly submerged below the rising CCD. We found that shoaling of the CCD since the industrial revolution has submerged 12,432,096 km^2 of ocean floor (3.60% of total ocean area) below the CCD. Further hypothetical shoaling of the CCD by 100 m increments illustrated that the surface area of seafloor submerged below the CCD has risen by 14% with 300 m of shoaling, such that 51% of the ocean area will be below the CCD. All categories of geomorphic feature mapped in one global database intersect the lysocline and will be (or already are) submerged below the CCD with much regional variation since the rise in CCD depth during the last 150 years varies significantly between different ocean regions. For seamounts, the highest percentages of increase in area submerged below the CCD occurred in the Southern Indian Ocean and the South West Atlantic regions (6.3% and 5.9%, respectively). For submarine canyons we found the South West Atlantic increased from 3.9% in pre-industrial times to 8.0% at the present time, the highest percentage of canyons found below the CCD in any ocean region.

We also carried out a relative risk assessment for future submergence of ocean floor below the CCD in 17 ocean regions. In our assessment we assumed that the change in CCD from pre-industrial times to the present is an indicator of the likelihood and the change in percentage of seafloor submerged below the CCD due to a hypothetical 300 m rise in the CCD is an indicator of the consequences. We found that the western equatorial Atlantic is at high risk and 9 other Ocean Regions are at moderate risk. Overall, geomorphic features in the Atlantic Ocean and southern Indian Ocean are at greater risk of impact from a rising CCD than Pacific and other Indian Ocean regions.

A separate analysis of the Arctic Ocean points to the possible submergence of glacial troughs incised on the continental shelf within a mid-depth (400–800 m) acidified water mass. We also found that the area of national Exclusive Economic Zones submerged below the rising CCD exhibits extreme variability; with 300 m of CCD shoaling we found a $>$ 12% increase in area submerged below the CCD for 23 national EEZs, whereas there was virtually no change for other countries.

1. Introduction

The "lysocline" is the transition zone in the ocean within which the calcium carbonate mineral "calcite" becomes unstable and begins to dissolve. Its upper limit is the calcite saturation depth (CSD) and its lower limit is the calcite (carbonate) compensation depth (CCD). Above

* Corresponding author.
E-mail address: Peter.Harris@grida.no (P.T. Harris).

https://doi.org/10.1016/j.margeo.2023.107121
Received 9 April 2023; Received in revised form 7 August 2023; Accepted 13 August 2023
Available online 15 August 2023

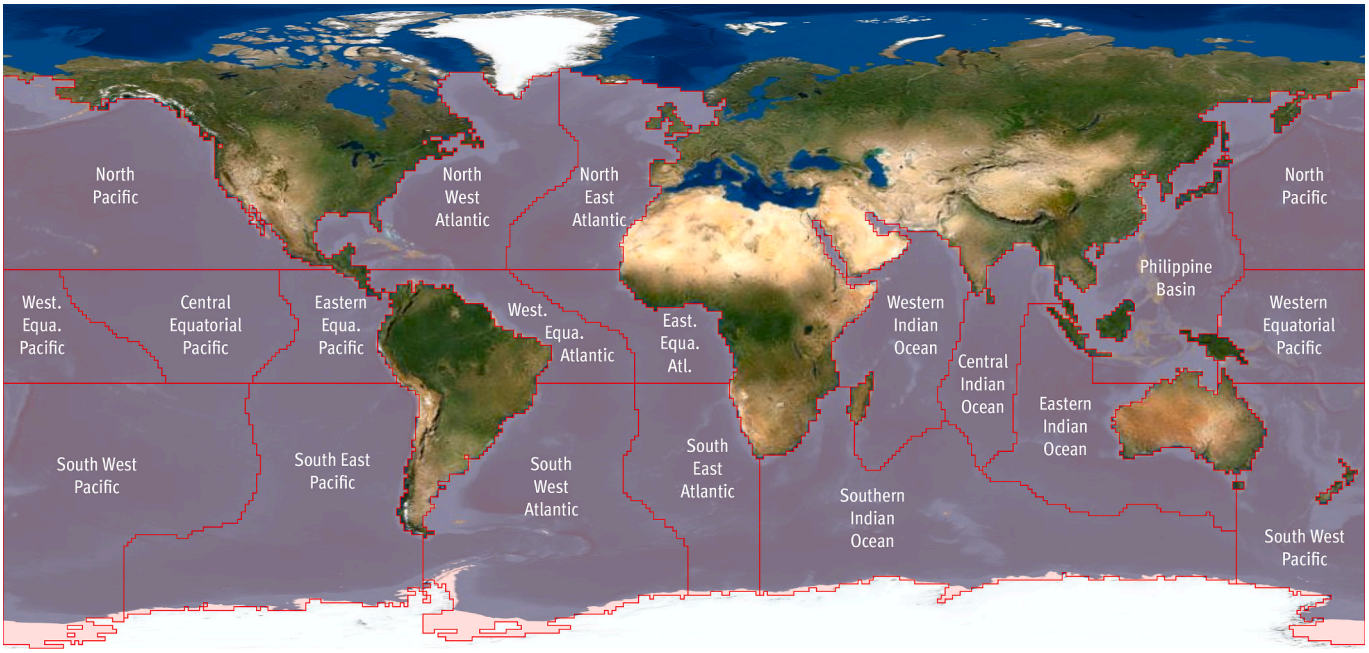

Fig. 1. Map showing the 18 ocean regions included in this study. The 17 regions mapped by Sulpis et al. (2018) were manually edited and clipped in ArcGIS to stretch all the ocean areas to the respective continents. The Arctic Ocean was included as a separate (18th) region; the Mediterranean Sea is not included.

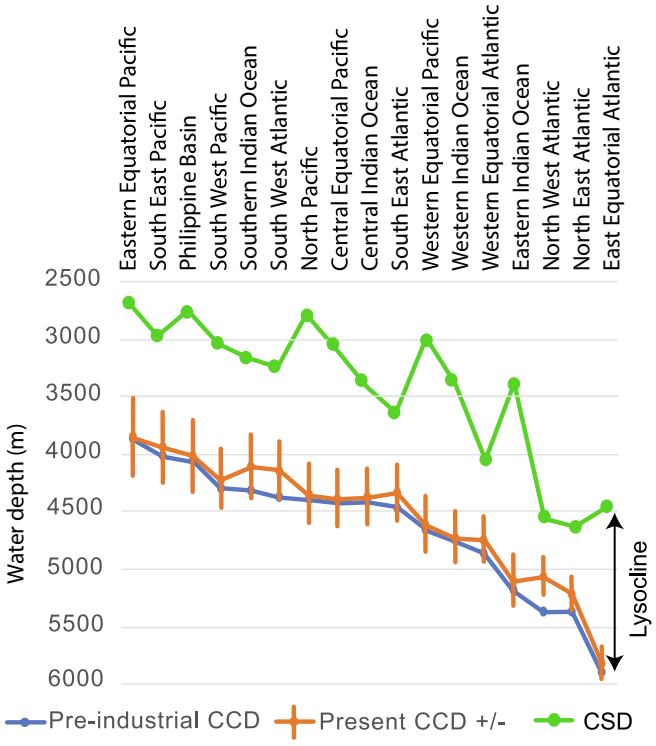

Fig. 2. Depth of the CCD modelled by Sulpis et al. (2018) showing pre-industrial and present CCD for the 17 ocean regions ranked in order of increasing, pre-industrial CCD. In general, the Pacific is more acidic (shallow CCD/CSD) than the Atlantic (deep CCD/CSD) but there is variability between ocean regions. Error bars for the present-day CCD (after Sulpis et al., 2018) are shown.

the CSD ocean water is super-saturated with calcite and seabed sediments are calcareous rich. Below the CCD seabed sediments contain little or no carbonate minerals, the carbonate "snow line" (Woosley, 2016). Sediments within the lysocline exhibit a decline in content of calcareous minerals with increasing depth (Sulpis et al., 2018).

Aragonite is another calcium carbonate mineral whose chemistry is less stable (and hence much more soluble) in seawater than calcite. The aragonite compensation depth (ACD) is therefore much shallower than the CCD. Aragonite accounts for about 50% of the calcium carbonate flux in the ocean (mainly the shells of marine snails called pteropods), essentially equal with the calcite flux (Manno et al., 2007). Sulpis et al. (2022) suggested that the dissolution of aragonite at the sea floor favours the preservation of less soluble calcite.

Due mainly to burning of fossil fuels, humans have caused atmospheric carbon dioxide content to rise to levels that have not occurred naturally over many millions of years. Carbon dioxide is being absorbed by the ocean where its chemical conversion to carbonic acid has already caused the surface ocean to become more acidic than it has been for at least the last 2 million years (Honisch et al., 2009). As a dissolved gas, CO_2 is carried to abyssal depths by the ocean conveyor where acidification is expected to cause the lysocline to rise (Archer et al., 1998), a process operating on a multi-century time scale.

Acidification of the oceans is acknowledged as a threat to ocean health in the United Nations Sustainable Development Goals (SDGs), Goal 14 to "Conserve and sustainably use the oceans, seas and marine resources for sustainable development" and SDG indicator 14.3.1: "Average marine acidity (pH) measured at agreed suite of representative sampling stations" (United Nations, 2023a). It is also a factor to consider in the design of any marine protected areas established in the high seas under the recently adopted UN Ocean Treaty (United Nations, 2023b), in which protection of deep sea biodiversity is a key goal (eg. Albright et al., 2023). In the absence of information on deep sea biodiversity, surrogates (Harris, 2012) such as ocean water properties and seafloor geomorphic features have been proposed (e.g., Harris and Whiteway, 2009; Sayre et al., 2017; Fischer et al., 2019). Here we first review recent modeling of the CCD and then study how seafloor morphology will affect the depth of the CCD under future climate change.

1.1. *Previous CCD modeling*

In their recent study, Sulpis et al. (2018) used a rate model to derive global benthic calcite dissolution rates for abyssal sediments in 17

Table 1
The percentage of the ocean regions' (Fig. 1) areas exposed below the CCD by hypothetical shoaling of the CCD. The rise in the CCD (m) with estimated error from Sulpis et al. (2018) was used to estimate the percentage below the pre-industrial CCD and the percentage area presently below the CCD. The percentage areas for +100 m, +200 m and + 300 m were estimated as explained in the methods. Total ocean area follows Sulpis et al. (2018), which excludes the Arctic Ocean and the Mediterranean Sea.

Ocean Region	Total Area km^2	Below CCD Pre-industrial times (%)	Below CCD Present (%)	Rise of CCD Pre-industrial to Present (m)	Below CCD Present +100 m (%)	Below CCD Present +200 m (%)	Below CCD Present +300 m (%)
1 Central Equatorial Pacific	16,580,040	45.70	47.63	20 ± 276	57.14	65.17	71.37
2 Central Indian Ocean	11,022,170	37.12	38.35	36 ± 261	42.15	45.90	49.08
3 East Equatorial Atlantic	10,156,820	0.55	0.948	73 ± 161	1.73	3.16	6.05
4 Eastern Equatorial Pacific	9,440,670	28.06	29.07	19 ± 331	34.52	40.70	47.32
5 Eastern Indian Ocean	18,149,390	22.23	25.59	80 ± 231	29.93	33.90	37.73
6 North East Atlantic	13,585,500	6.10	10.65	149 ± 178	13.81	16.91	19.89
7 North Pacific	42,585,460	66.37	67.11	36 ± 293	69.13	71.01	72.76
8 North West Atlantic	18,237,390	13.20	23.33	316 ± 185	26.39	29.38	32.18
9 Philippine Basin	20,110,530	32.15	32.57	30 ± 316	33.98	35.23	36.39
10 South East Atlantic	13,512,790	44.15	49.12	133 ± 251	52.61	55.98	59.41
11 South East Pacific	24,878,730	43.39	47.78	69 ± 308	54.05	59.75	65.06
12 South West Atlantic	23,764,040	38.25	46.11	227 ± 280	49.59	52.74	55.60
13 South West Pacific	45,292,370	42.48	45.21	81 ± 287	48.50	51.62	54.50
14 Southern Indian Ocean	27,405,630	36.27	46.24	216 ± 288	50.05	53.51	56.78
15 Western Equatorial Atlantic	9,520,260	22.49	27.11	129 ± 215	30.79	34.75	39.28
16 Western Equatorial Pacific	23,555,170	49.39	50.42	30 ± 269	53.53	56.66	59.89
17 Western Indian Ocean	17,104,860	12.31	12.77	18 ± 245	15.92	19.76	23.48
TOTAL (Average)	344,901,850	36.91	40.51	97.8 ± 257	44.13	47.61	50.91

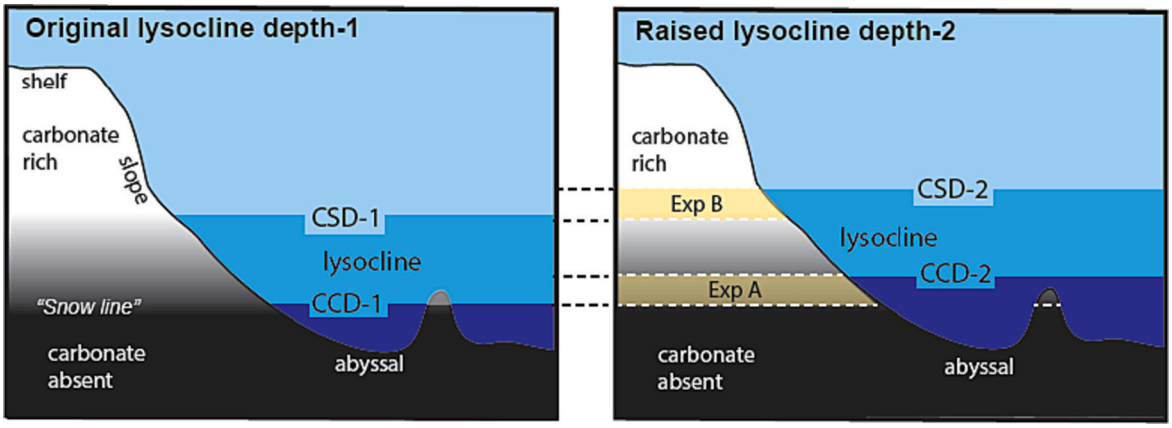

Fig. 3. Conceptual diagram showing two seafloor areas A and B exposed by the rising lysocline. The carbonate content of seafloor sediments decreases within the lysocline, reaching zero below the CCD (carbonate "snow line"). The present study focuses on areas previously above the CCD but now below it (Exp-A), noting that areas previously above the CSD but now within the lysocline (Exp-B) will also be effected by acidification of the oceans.

separate ocean regions (Fig. 1). The depth of the CCD in pre-industrial times was estimated to range from as shallow as 3895 ± 377 m in the eastern equatorial Pacific to as deep as 5926 ± 155 m in the eastern equatorial Atlantic (Fig. 2). The depth of the CCD varies with the length of time since the bottom water has been exposed to the surface (bottom water "age"). Over time, benthic respiration and oxidation of organic matter add CO_2 such that the oldest water masses have the highest concentrations of CO_2 and therefore the shallowest CCD. The youngest bottom water is formed in locations of downwelling (e.g., adjacent to the polar seas) and the CCD is deeper (e.g., Broecker, 1991; Schmitz and McCartney, 1993; Johnson, 2008).

Changes in the depth of the CCD from pre-industrial times to its present position (estimated for 2002) range from a rise (shallowing) of 316 ± 185 m in the North West Atlantic above its pre-industrial depth of ~5400 m, to 18 ± 245 m (essentially no change) in the western Indian Ocean. The average rise in the CCD across all ocean areas was estimated

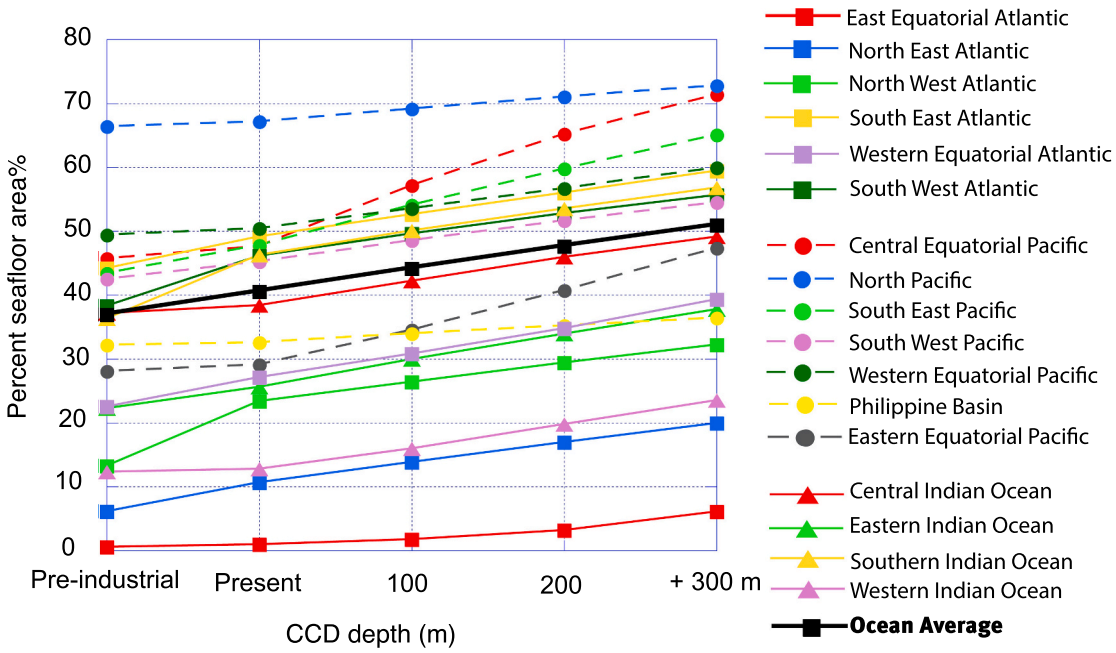

Fig. 4. The changes in percent area of ocean exposed to corrosive bottom waters in 17 different ocean regions in pre-industrial times (−100 m), at present and resulting from a hypothetical shoaling of the CCD in three, 100 m increments. The slope of lines gives a relative indication of change in area below the CCD with CCD shoaling. Estimated error (not shown) for present CCD is as per Table 1.

to be about 98 ± 257 m since pre-industrial times, with considerable spatial heterogeneity in the modelled shoaling of the CCD (Fig. 2; Sulpis et al., 2018). In general, the greatest change in CCD since post-industrial times occured in areas of downwelling, where the bottom water was youngest (Fig. 2) and this was attributed by Sulpis et al. (2018) to the post-industrial addition of CO_2 to the atmosphere. Although the large error bars in the estimated CCD depths were acknowledged (Fig. 2 and Table 1), it was concluded by Sulpis et al. (2018) that there has been a general rise in the CCD since pre-industrial times which has been causing an increased rate of carbonate sediment dissolution (i.e., a rise in the carbonate sediment "snow line") amounting to 40–100% of the total seafloor dissolution at its most intense locations.

The thickness of the lysocline (difference in depth between CCD and CSD) averages around 1081 m over all ocean regions (Fig. 2). However, there is considerable spatial variation in estimated lysocline thickness between ocean regions, ranging from 536 ± 185 m in the Northwest Atlantic to 1755 ± 231 m in the Eastern Indian Ocean. Lysocline thickness exhibited no significant difference between pre-industrial times and the present day with an average increase of 15.6 m (within the error limits for available data; see Sulpis et al., 2018).

Palaeoceanographers have reported that oceanic acidification events have happened before in the geologic past, the most recent occurring in association with the Palaeocene-Eocene Thermal Maximum (PETM; 55.8 million years ago). This global warming event was short-lived (~200,000 years) during which temperatures increased by 5–9 °C and the Atlantic CCD shoaled to <2000 m (Zachos et al., 2005). It was also marked by the largest deep-sea mass extinction among calcareous benthic foraminifera in the last 93 million years (Thomas, 1998). Although the unprecedented rapid pace of change in the environment during the Anthropocene limits the applicability of the fossil record to inform what we may expect in the coming decades to century (Kump et al., 2009), the available information indicates that human-induced ocean acidification will impact oceanic ecosystems, although how significantly remains unknown.

The rising depth of the lysocline will change the chemical environment of benthic organisms inhabiting depths that were previously above the lysocline and are now within it as well as organisms that existed within the lysocline but find themselves below it. Depending on their sensitivity to these undersaturated conditions, benthic fauna will either remain and adapt to the changed conditions, or their distribution will shallow as they die out in, or otherwise avoid colonizing, areas that they cannot tolerate. The literature on the exact response of deep sea fauna to the effects of acidification are mainly speculative due to the lack of data (Fabry et al., 2008; Widdicombe and Spicer, 2008; Hofmann et al., 2010). The acidification of the abyssal zone is believed to favour agglutinated foraminifera over calcifying species, for example. However, studies have focused on carbonate chemistry and its effect of dissolution of plankton shells (Milliman et al., 1999). A recent paper by Simon-Lledó et al. (2023) has provided the first evidence that the CCD is a biological boundary located between 4300 and 4800 m depth in the Clarion-Clipperton zone of the northeast Pacific. The authors found that there was no change in indicators of species diversity across the CCD but rather that species that build a carbonate shell were absent below the CCD and were replaced by other, non-calcifying species.

A key consideration is that the acidification of the deep ocean is likely to occur in combination with a decrease in dissolved oxygen, decreased POC flux and a weakening of abyssal currents, all attributed to climate change (Sweetman et al., 2017). To these climate change related pressures we must add the impacts of pollution (e.g., plastic pollution; Galgani et al., 2022) and other human activities such as fishing, cable laying and seismic surveys among others (Harris, 2020). These cumulative impacts acting together will have a greater impact on benthic biodiversity than any one pressure acting in isolation (Halpern et al., 2008).

There is a popular misconception that carbonate minerals will dissolve and buffer the acidification effect of increased anthropogenic CO_2. While this is correct over geologic (~1000 year) timescales, there is a time lag involved that is often overlooked as explained by Archer et al. (1998) and Andersson and Mackenzie (2012). Over timescales of human lifespans, the buffering effect is minimal. Therefore, the recent ~100 m rise in the CCD since pre-industrial times reported by Sulpis et al. (2018) is likely to continue this century. Further, the rate of rise of the CCD is likely to accelerate in the next century as the ocean conveyor delivers increasingly higher concentrations of dissolved carbon dioxide into the deep ocean.

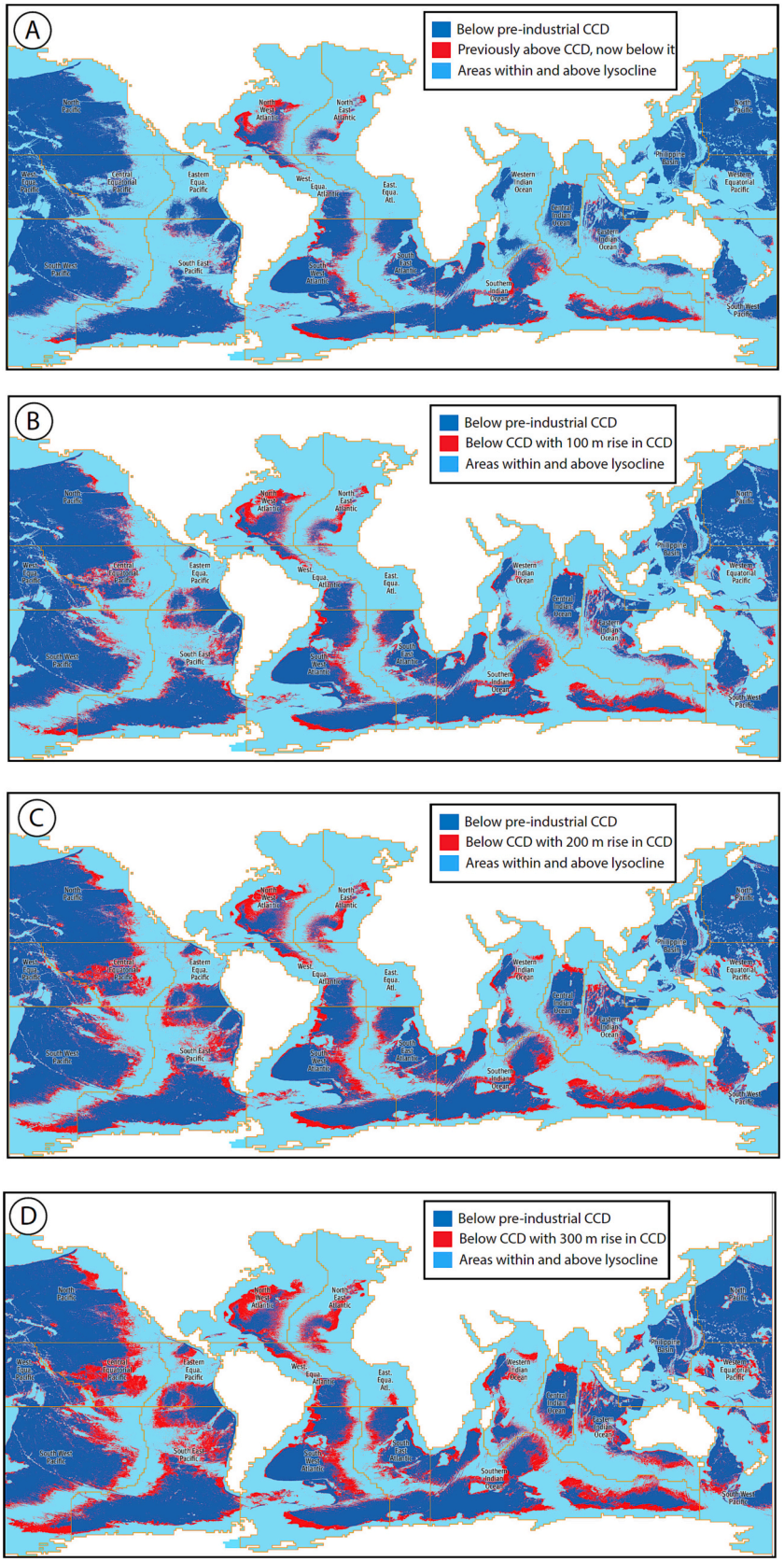

Fig. 5. Maps showing the changes in area of ocean exposed to corrosive bottom waters in 17 different ocean regions, showing area below pre-industrial CCD (dark blue), above lysocline (light blue) and expanding below CCD (red), where: (A) present day; (B) with additional 100 m hypothetical shoaling of CCD; (C) with 200 m hypothetical shoaling of CCD; (D) with 300 m hypothetical shoaling of the CCD. Since the future CCD depth will be determined by deep ocean circulation and changes in ocean chemistry, these maps do not represent a time series, but rather only show changes in area with hypothetical shoaling of the CCD. (For interpretation of the references to colour in this figure legend, the reader is referred to the web version of this article.)

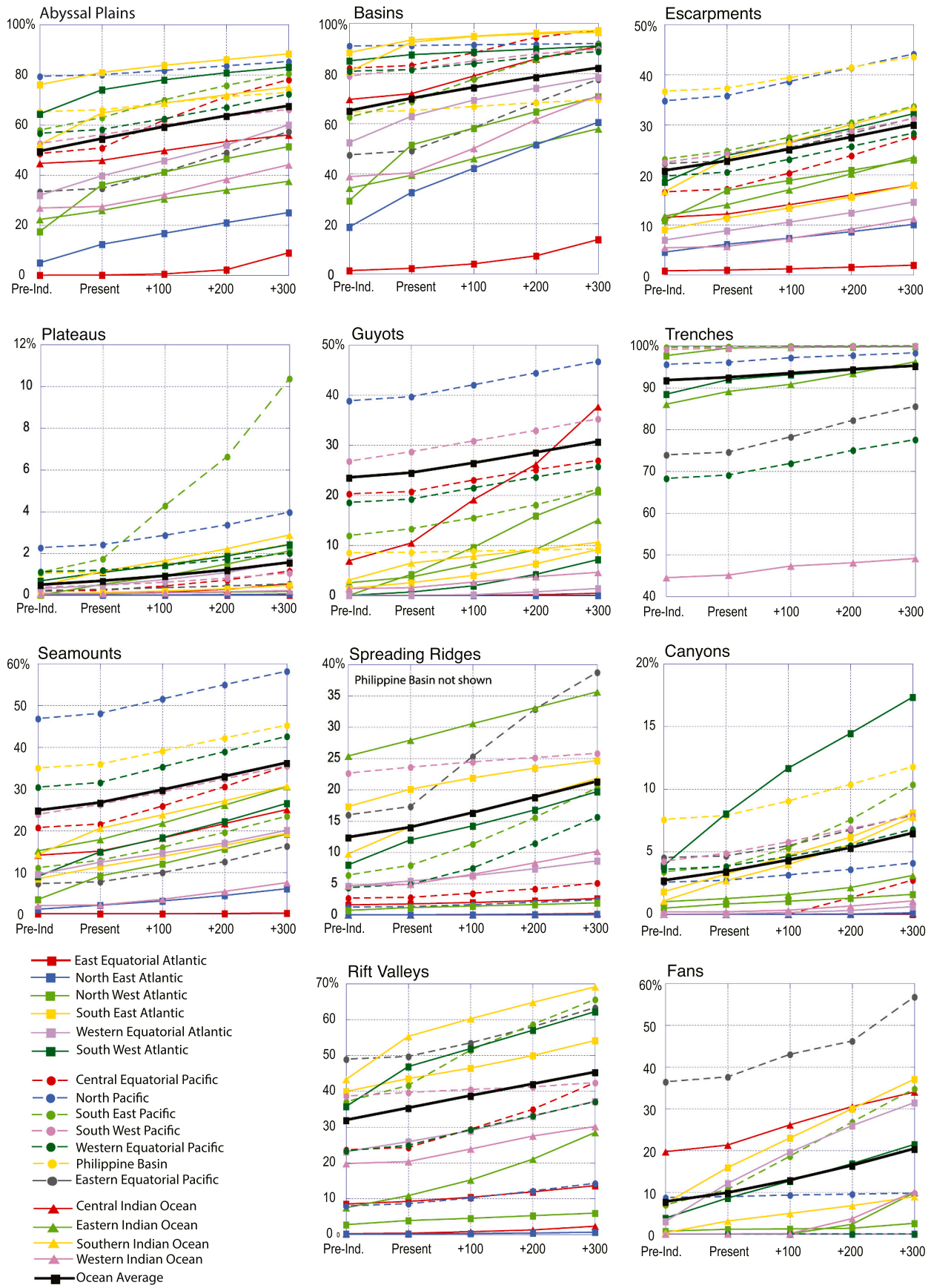

Fig. 6. Percent surface areas of selected geomorphic feature types versus hypothetical future shoaling of the CCD in 100 m increments. Note the Y-axes (percentage feature area) are plotted on different scales.

Table 2
Change in area of geomorphic features located below the CCD in km^2 (percentage shown in brackets) at the present time in relation to pre-industrial times listed for 17 ocean regions shown in Fig. 1 and for the total global ocean. Largest percent change indicated by shaded numbers. NP = not present.

Region	Abyssal Plain km^2	Basin km^2	Canyon km^2	Fan km^2	Plateau km^2	Escarp. km^2	Seamount km^2	Guyot km^2	Spreading Ridge km^2	Rift Valley km^2	Trench km^2
1. C Eq Pacific	220,412 (2.26%)	29,833 (1.07%)	0	NP	20 (<0.1%)	1980 (0.59%)	2080 (0.81%)	60 (0.46%)	100 (0.1%)	50 (0.67%)	NP
2. C Indian	46,614 (1.2%)	134,832 (2.29%)	0	40,900 (1.6%)	90 (0.01%)	2200 (0.65%)	780 (0.99%)	40 (3.56%)	10 (<0.1%)	10 (0.11%)	NP
3. E Eq Atlantic	1229 (0.05%)	40,433 (0.89%)	0	0	0	590 (0.13%)	0	0	290 (0.14%)	180 (0.7%)	NP
4. E Eq Pacific	41,765 (1.26%)	95,416 (1.71%)	80 (0.12%)	290 (1.17%)	40 (<0.1%)	2040 (0.47%)	470 (0.45%)	NP	6890 (1.33%)	260 (0.79%)	890 (0.71%)
5. E Indian	205,141 (3.6%)	611,304 (5.14%)	390 (0.24%)	0	640 (0.05%)	17,100 (2.22%)	7470 (2.69%)	90 (1.17%)	2060 (2.53%)	370 (3.36%)	2740 (3.06%)
6. NE Atlantic	217,614 (8.43%)	618,129 (14.0%)	0	0	10 (<0.1%)	15,180 (1.61%)	1880 (0.98%)	0	20 (<0.1%)	20 (0.04%)	NP
7. N Pacific	83,039 (0.63%)	18,660 (0.10%)	530 (0.18%)	510 (0.24%)	640 (0.15%)	29,680 (1.04%)	21,980 (1.26%)	3360 (0.84%)	170 (0.11%)	140 (0.64%)	1650 (0.61%)
8. NW Atlantic	853,607 (20.9%)	1,848,230 (22.5%)	1200 (0.37%)	1120 (0.46%)	2950 (0.51%)	74,410 (6.11%)	11,210 (5.68%)	170 (4.2)	640 (0.47%)	260 (1.19%)	2080 (1.79%)
9. Philip. Basin	8296 (0.75%)	37,722 (0.47%)	1670 (0.32%)	0	610 (0.1%)	15,530 (0.62%)	4370 (0.92%)	10 (0.06%)	4060 (1.12%)	360 (0.76%)	130 (0.03%)
10. SE Atlantic	135,455 (4.87%)	319,316 (4.98%)	2490 (1.39%)	23,050 (8.60%)	170 (0.08%)	16,280 (2.34%)	10,390 (2.90%)	490 (1.14%)	9600 (2.77%)	1250 (3.58%)	NP
11. SE Pacific	391,892 (5.03%)	1,083,490 (6.28%)	720 (0.43%)	7210 (3.69%)	1160 (0.65%)	20,070 (1.65%)	9700 (1.82%)	460 (1.35%)	14,280 (1.57%)	2870 (4.58%)	360 (0.16%)
12. SW Atlantic	695,703 (9.69%)	241,089 (2.45%)	11,760 (4.14%)	27,290 (4.80%)	4120 (0.41%)	56,260 (5.33%)	11,190 (5.89%)	390 (0.67)	27,690 (3.99%)	7580 (11.17%)	3520 (3.48%)
13. SW Pacific	365,583 (3.53%)	478,147 (2.75%)	2340 (0.63%)	NP	5120 (0.09%)	45,850 (1.71%)	28,430 (2.31%)	2050 (1.88%)	7030 0.97%)	790 (1.00%)	720 (0.26%)
14. S Indian	1,313,843 (12.58%)	1,290,078 (11.64%)	5400 (1.61%)	15,030 (2.81%)	14,790 (0.70%)	65,250 (6.59%)	16,130 (6.27%)	770 (3.4%)	25,960 (4.30%)	6690 (12.01%)	NP
15. W Eq Atlantic	180,723 (7.79%)	427,251 (10.46%)	40 (0.03%)	55,000 (9.09%)	560 (0.16%)	10,390 (1.87%)	4960 (2.89%)	0	2260 (0.82%)	1050 (2.81%)	NP
16. W Eq Pacific	80,709 (1.51%)	67,839 (0.71%)	390 (0.23%)	NP	1420 (0.07%)	17,100 (0.74%)	13,590 (1.13%)	830 (0.67%)	890 (0.56%)	360 (1.57%)	1650 (0.81%)
17. W Indian	26,542 (0.63%)	78,603 (1.45%)	60 (0.02%)	0	70 (<0.1%)	2840 (0.26%)	530 (0.18%)	70 (0.19%)	1680 (0.23%)	470 (0.54%)	200 (0.63%)
Total	4868,691 (4.98%)	7,420,959 (4.90%)	27,110 (0.71%)	170,430 (2.14%)	32,410 (0.19%)	392,880 (1.91%)	145,200 (1.86%)	8800 (0.95%)	103,610 (1.61%)	22,700 (3.36%)	13,860 (0.71%)

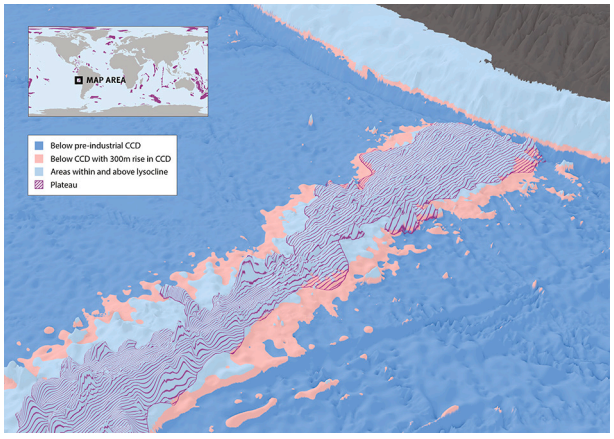

Fig. 7. Three-dimensional diagram illustrating how a projected 300 m rise in CCD will result in a rise in the "snow line" with more of the Nazca Ridge (plateau) area being located below the CCD.

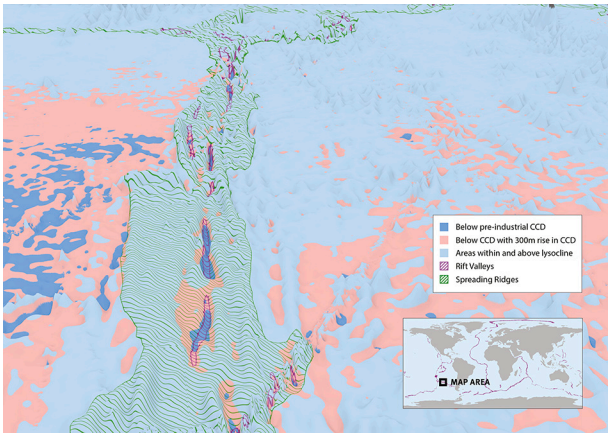

Fig. 8. Three-dimensional diagram illustrating how a projected 300 m rise in CCD will result in a rise in the "snow line" with more rift valley area being located below the CCD on the SE Pacific spreading ridge.

1.2. Special situation of the Arctic Ocean

The analysis of water and seabed sediment samples indicate that the deep abyssal seafloor of the Arctic Ocean lies wholly above the CCD (Jutterström and Anderson, 2005). Modeling suggests that deep water masses in the Arctic are not expected to become under-saturated with calcium carbonate within this century. Recent observations indicate that the acidification of the Arctic Ocean is occurring four times faster than other ocean regions, linked to reduction in sea ice cover (Qi et al., 2022). However, the models also predict an interesting effect of intruding Atlantic Ocean water masses transporting carbonate undersaturated water into mid-depth regions of the Arctic (Luo et al., 2016; Terhaar et al., 2020). In addition to the importation of carbonate undersaturated water into the Arctic from the North Atlantic there is the potential added impact of methane seepage from melting of seafloor gas hydrates and permafrost within the Arctic basin (Biastoch et al., 2011; GRID-Arendal,

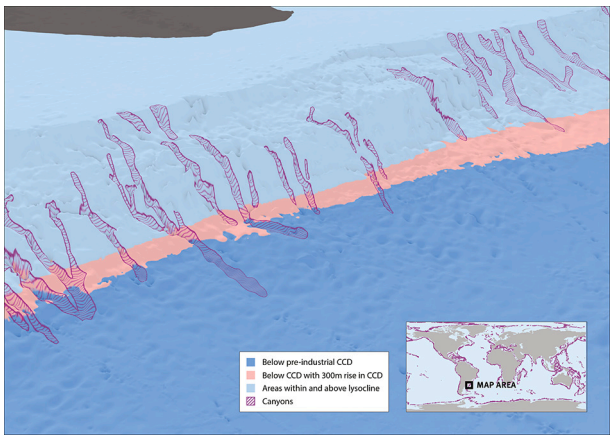

Fig. 9. Three-dimensional diagram illustrating how a projected 300 m rise in CCD will result in a rise in the "snow line" with more canyon area being located below the CCD adjacent to the Argentina continental slope.

2020; El bani Altuna et al., 2021). Hence, although shoaling of the deep water lysocline is not expected to expose any deep seafloor habitats to undersaturated carbonate waters this century, it is rather the mid-depth waters in the Arctic, within the 400–800 m depth range (Terhaar et al., 2020), that will potentially be impacted.

1.3. Aims and objectives

We ask what ocean areas, which geomorphic features and which nations will be impacted in the next century by the rising lysocline, by mapping the area of seafloor that will be exposed to more corrosive ocean water as a result of increased anthropogenic CO_2 dissolved in seawater and attendant rising of the CCD. We will focus on the area of seabed that was previously located within the lysocline, immediately above the CCD, but which is now below it and exposed to corrosive bottom waters (i.e., area Exp-A in Fig. 3). Our objective is to better understand which geographic regions and what categories of geomorphic features are most at risk in order to inform better decision-making in ocean governance.

2. Methods

2.1. Calculation of ocean regions and their exposure to shoaling CCD

Global data on the depth of carbonate compensation depth (CCD) and calcite saturation depth (CSD) were tabulated in Sulpis et al. (2018) for 17 different ocean regions (Fig. 1). We mapped the pre-industrial and modern (circa 2002) depths of the CSD and CCD (from Sulpis et al., 2018) in ArcGIS using the bathymetric depth contours from a recent global bathymetry map (Tozer et al., 2019). The surface area located between these two isobaths in each of the 17 ocean regions was then measured and mapped in GIS.

Based on the modern CCD, we assume an increase in elevation of the CCD in three 100 m increments and mapped the affected seafloor area (for 100, 200 and 300 m rises in CCD). These increments were subjective and hypothetical but reflect general expectations in the extent that the CCD will shoal within this century (Archer et al., 1998; Sulpis et al., 2018), noting that the current depth of the CCD is not known to within <200 to 300 m depth in most ocean regions (Fig. 2; Table 1). The amount of shoaling that has occurred since pre-industrial times (albeit poorly constrained) varies significantly between ocean regions (Fig. 2) and hence it is expected that the CCD shoaling will occur at different rates in different regions, faster in areas of downwelling and much slower (taking probably many centuries) in other regions.

All the SRTM15 tiles from Tozer et al. (2019) were merged to create a global bathymetry data layer at 15 arc *sec* (approximately 500 × 500 m at the equator) resolution. The global bathymetry raster was clipped to each ocean area to create 17 individual SRTMs for each ocean polygon. This step was mostly done to increase the analysis speed of the subsequent classification of ocean depths. Each of the raster tiles for each ocean area was reclassified four times to identify: (A) the depth between pre-industrial and present CCD; (B) present CCD + 100 m; (C) present CCD +200 m; and (D) present CCD + 300 m. Surface areas were then calculated using the world Cylindrical Equal Area projection.

For the Arctic there is a special situation whereby acidification is projected to intersect the depth range 400–800 m, as proposed by Terhaar et al. (2020). Thus, in Step 1 we replaced the elevation of the CCD in depth increments and with this specific depth range in GIS. For Steps 2 and 3, we used the same approach as above within the 400–800 m depth range.

2.2. Geomorphic features

Using GIS, we overlaid the derived bathymetry polygons (A-D as defined above) with the global seafloor geomorphic features (GSFM) database of Harris et al. (2014) to create inventories of features exposed, their numbers and surface areas for each ocean basin. Each of the outputs from the geomorphic layers pairwise intersect with each individual CCD layer were merged together to create 4 final polygon layers. Given the 30 arc sec, or approximately 1 km, grid resolution of the SRTM30_PLUS bathymetric model of Becker et al. (2009) used by Harris et al. (2014) to map geomorphic features, the location of the derived feature boundaries will reflect this resolution. Assuming the precision of interpretation of the bathymetric model is 3 × 3 grid cells in any dimension, Harris et al. (2014) rounded all area estimations to the nearest 10 km^2 which is adopted in this study.

2.3. National Exclusive Economic Zones and the rising CCD

We overlaid the derived bathymetry polygons (A-D as defined above) with national Exclusive Economic Zones (EEZs) from VLIZ 2022? to create inventories of features exposed, their numbers and surface areas for each country. Each of the outputs from the geomorphic layers pairwise intersect with each individual CCD layer were merged together to create four final polygon layers to the nearest 10 km^2 as explained above.

3. Results

3.1. Ocean areas below the CCD

For the 17 ocean regions included in the Sulpis et al. (2018) analysis (excluding the Arctic Ocean) our analysis indicated that around 37% (127,303,272 km^2) of the global ocean floor lies below the pre-industrial depth of the CCD. Shoaling of the CCD since the industrial revolution has submerged an additional 12,432,096 km^2 of ocean floor (3.6% of total ocean area) below the CCD. Conceptually, this is the area "Exp. A" as illustrated in Fig. 3. Thus, at present, 40.5% of the ocean floor (139,685,248 km^2) is submerged below the CCD.

Further hypothetical shoaling (shallowing) of the CCD by an increment of 100 m illustrates that the surface area of seafloor submerged below the CCD (Exp. A; Fig. 3) rises by 24,947,550 km^2 equal to 7.2% of total ocean area. An additional 48,298,879 km^2 equal to 14.0% of total ocean area is submerged below the CCD with 300 m of CCD shoaling, referenced to the pre-industrial depth of the CCD (Table 1). Thus, if the CCD shoals by 300 m then 51% of the ocean seafloor area will be deeper than the CCD.

There is much heterogeneity in the areas below the CCD between the different ocean regions (Fig. 4). The area below the CCD in pre-industrial times is estimated here to have ranged from 0.55% to 66% of ocean regions, which is a significant difference even allowing for the large

Table 3
Feature areas mapped in this study as below the pre-industrial CCD as defined by Sulpis et al. (2017).

Ocean Region	Abyssal Hills (km^2)	Abyssal Mountains (km^2)	Bridges (km^2)	Hadal (km^2)	Rise (km^2)	Slope (km^2)	Sill (km^2)	Terrace (km^2)	Trough (km^2)
1 Central Equatorial Pacific	2,525,430	308,980		5100		100			
2 Central Indian Ocean	2,077,120	289,760	90	210	503,750		10		37,900
3 East Equatorial Atlantic	24,960	8090		22,620					
4 Eastern Equatorial Pacific	1,275,200	209,300	300	10,670		48,880			4450
5 Eastern Indian Ocean	2,049,870	503,010	770	214,960	47,940	4780			47,620
6 North East Atlantic	442,590	200,630		38,920	57,380				1060
7 North Pacific	12,190,340	3,731,270	690	147,990	45,750	140,690		6060	97,760
8 North West Atlantic	1,057,500	320,680	30	232,500	38,290	790			4200
9 Philippine Basin	2,907,060	2,116,010	980	578,200		135,400	230	500	147,370
10 South East Atlantic	3,199,360	647,910		720	369,440	860			
11 South East Pacific	5,340,510	837,210	410	51,340	866,100	53,160			
12 South West Atlantic	3,303,530	959,980	130	202,490	2,658,650	7120	300		62,110
13 South West Pacific	11,347,360	2,175,680	390	223,600	216,590	50,900	980		73,290
14 Southern Indian Ocean	3,686,540	805,460		3100	1,319,200	1810	20		
15 West Equatorial Atlantic	1,107,790	289,760		3430	359,600	30			
16 Western Equatorial Pacific	5,918,600	2,275,240	380	352,880		53,340	170	630	193,000
17 Western Indian Ocean	686,200	279,780	30	940	61,100	970			5280
TOTAL Area Below CCD	59,139,970	15,958,740	4210	3,421,620	6,543,780	498,810	1704	7200	674,030
Total Area	146,153,780	54,859,300	7830	3,425,890	28,487,930	17,142,750	37,358	1,992,850	2,566,490

errors in the estimate of CCD depth (Table 1; Sulpis et al., 2018). The average pre-industrial percentage area below the CCD of the 17 areas is 31.7 +/− 17.2 (standard deviation). The North Pacific had the largest area below the CCD before the industrial revolution at 66%, rising to about 73% with 300 m of hypothetical CCD shoaling (Fig. 4). The East Equatorial Atlantic had the smallest percentage area below the CCD before the industrial revolution at 0.55%. With 300 m of hypothetical CCD shoaling the area below the CCD increases to only 6%, the smallest area below the CCD of any ocean region. The North East Atlantic has the second smallest area below the CCD at 6.1%, which increases to about 20% with 300 m of hypothetical CCD shoaling (Fig. 4).

The change in seafloor area below the CCD between pre-industrial times and the present was greatest for the Northwest Atlantic, the Southwest Atlantic and the Southern Indian Ocean (Fig. 5A). As noted above, the 200 to 300 m rise in CCD in these areas is attributed by Sulpis et al. (2018) to strong downwelling of oceanic water masses containing increased concentrations of dissolved CO_2 compared with pre-industrial times. The changes in CCD correspond with ocean areas of between 8.59% and 11.09% (well above the global average of 3.56%) that have become submerged below the CCD since the industrial revolution. These areas increase to between 19.24% and 20.77% with 300 m of hypothetical shoaling of the CCD (Figs. 4 and 5).

Four ocean regions had <1% increases in area submerged below the CCD between pre-industrial and present: the Eastern Equatorial Atlantic (0.40%); Philippine Basin (0.42%) Western Indian Ocean (0.46%) and the North Pacific (0.74%). These regions are distant from locations of downwelling water masses and presumably have relatively "old" bottom water in comparison with other ocean regions.

3.2. Geomorphic features submerged below the CCD

All categories of off-shelf seafloor geomorphic features mapped by Harris et al. (2014) were found to intersect the depth-range of the lysocline in several (if not all) ocean regions in the present study. These extended from the deepest hadal features (e.g., ocean trenches) to features extending onto the continental slope (submarine canyons and fans; Fig. 6). In general, there was great variability between ocean regions in terms of the percentages of features submerged below the CCD in pre-industrial and present times and also the areas predicted to be submerged by future CCD shoaling (Table 2; Fig. 6; Supplementary Table 1).

Vertically extensive features, like escarpments, guyots, seamounts and submarine canyons, partially intersected with the depth range of the rising CCD (e.g., Fig. 3). Only the deepest parts of canyons and fans extended below the CCD, hence their pre-industrial areas below the CCD were on average <10% (Fig. 6). The effect of shoaling of the CCD could result in some features coming into contact with the CCD for the first time; this can be seen for guyots, spreading ridges, submarine fans and canyons (Fig. 6). In such cases, the deepest parts of features occurred below the CCD after it has shoaled sufficiently; this is illustrated in Fig. 6 as a line emerges mid-way along the X-axis representing the first occurrence of a feature in that ocean region to extend below the depth of the CCD.

In contrast, >90% of the deep-water trenches were already below the CCD in pre-industrial times (Fig. 6). For abyssal plains and basins the figures were around 50 to 60% on average (Fig. 6). Seamounts, guyots, escarpments, and rift valleys all had between 20 and 30% of their areas submerged below the CCD in pre-industrial times (Fig. 6). The changes in CCD affecting each category of geomorphic feature are described in the following sections.

3.2.1. Abyssal plains

The area of abyssal plains in the 17 ocean regions is 97,843,544 km^2. A total of 49% of abyssal plains were submerged below the pre-industrial CCD and this has increased to 54.3% at the present time. The North Pacific and South East Atlantic had the largest areas submerged below the CCD at 79.3% and 76.3%, respectively in pre-industrial times and 80.0% and 80.9% at present. In contrast, the Eastern Equatorial Atlantic had only 0.01% submerged below the pre-industrial CCD increasing to 0.05% at present. With 300 m of hypothetical CCD shoaling, the average area of abyssal plains submerged is predicted to increase from 54.3% at present to 67.4% (Fig. 6).

The highest percentages of increase in area submerged below the CCD since pre-industrial times (steepest slopes in Fig. 6) occurred in the Northwest Atlantic and Southern Indian Ocean regions (20.9% and 12.6%, respectively). A smaller (<1%) increase in surface area occurred in the East Equatorial Atlantic, North Pacific and the Philippine Basin.

Table 4
List of geomorphic features projected to be submerged within the 400–800 m depth range of a hypothetical intrusion of an acidified mid-depth water mass in the Arctic Ocean as proposed by Terhaar et al. (2020). Features listed in decreasing order of percent area submerged.

Feature	Area	In 800–400 depth zone	
	(km^2)	(km^2)	%
Terrace	146,870	41,590	28.32
Glacial Trough	1,107,880	241,330	21.78
Slope	642,390	116,140	18.08
Shelf	3,849,470	368,330	9.57
Plateau	778,390	72,540	9.32
Canyon	328,930	16,920	5.14
Ridge	74,820	2890	3.87
Escarpment	146,430	3950	2.69

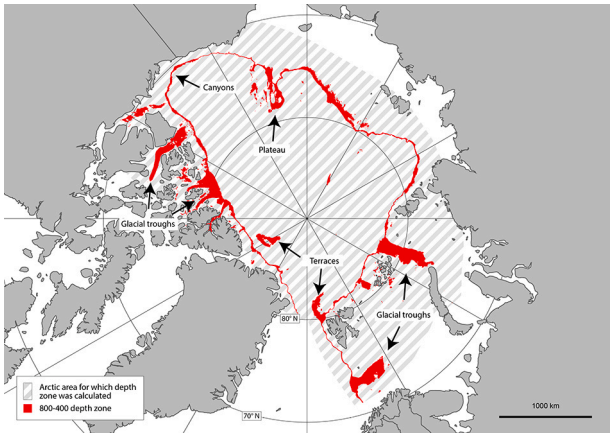

Fig. 10. Map showing the area (in red shading) impacted by the hypothetical intrusion of an acidified water mass into the central Arctic Ocean and affecting the 400 to 800 m depth range. Locations of some large areas of glacial troughs, terraces, plateaus and canyons are indicated. (For interpretation of the references to colour in this figure legend, the reader is referred to the web version of this article.)

3.2.2. Basins

The area of basins in the 17 ocean regions is 151,588,990 km^2. A total of 64.9% of basins were submerged below the pre-industrial CCD and this has increased to 69.8% at the present time. The North Pacific and South West Atlantic had the largest areas submerged below the CCD at 90.9% and 84.9%, respectively in pre-industrial times and 91.0% and 87.3% at present. North Pacific basins were also found at the greatest water depths of over 5300 m (Harris and Macmillan-Lawler, 2017). In contrast, the Eastern Equatorial Atlantic had only 1.2% submerged below the pre-industrial CCD increasing to 2.1% at present. With 300 m of hypothetical CCD shoaling, the average area of basins submerged was predicted to increase from 69.8% at present to 81.9% (Fig. 6).

The highest percentages of increase in area submerged below the CCD from pre-industrial times to the present (steepest slopes in Fig. 6) occurred in the North West Atlantic, North East Atlantic and Southern Indian Ocean regions (22.3%, 13.9 and 11.6%, respectively). A smaller (<1%) increase in surface area occurred in the East Equatorial Atlantic, North Pacific, Western Equatorial Pacific and the Philippine Basin.

3.2.3. Escarpments

Escarpments cover 20,524,040 km^2, of which on average 20.7% were submerged below the CCD in pre-industrial times increased to 22.7% at the present time. The Philippine Basin and North Pacific had the greatest areas below the pre-industrial CCD at 36.6% and 34.7%, respectively, which has increased to 37.3% and 35.8%, respectively, at the present time. In contrast, the Eastern Equatorial Atlantic had only 0.82% submerged below the pre-industrial CCD and increased to 0.96% at present. With 300 m of hypothetical CCD shoaling, the average area of escarpment submerged was predicted to increase from 22.7% at present to 29.9% (Fig. 6).

The highest percentages of increase in area of escarpment submerged below the CCD from pre-industrial times to the present (steepest slopes in Fig. 6) occurred in the Southern Indian Ocean, North West Atlantic and South West Atlantic, regions (6.6%, 6.0% and 5.3%, respectively). A smaller (<0.5%) increase in surface area occurred in the East Equatorial Atlantic, Western Indian Ocean and Eastern Equatorial Pacific.

3.2.4. Seamounts

Seamounts cover 7,814,770 km^2, and on average 24.8% of seamount area was submerged below the CCD in pre-industrial times, increasing to 26.6% at the present time. For reference, Harris et al. (2014) mapped 9951 seamounts in the world ocean having an average area of 790 km^2 (see also Costello et al., 2010; MacMillan-Lawler and Harris, 2016). The North Pacific and Philippine Basin had the greatest areas below the pre-industrial CCD at 46.8% and 35.0%, respectively, which has increased to 48.1% and 35.9%, respectively, at the present time. In contrast, the Eastern Equatorial Atlantic had only 0.08% of seamount area submerged below the pre-industrial CCD with no change up to the present. With 300 m of hypothetical CCD shoaling, the average area of seamount submerged was predicted to increase from the present 26.6% to 36.2% (Fig. 6).

The highest percentages of increase in area of seamount submerged below the CCD from pre-industrial times to the present (steepest slopes in Fig. 6) occurred in the Southern Indian Ocean and the South West Atlantic, regions (6.3% and 5.9%, respectively). A smaller (<0.5%) increase in surface area occurred in the East Equatorial Atlantic, Western Indian Ocean and Eastern Equatorial Pacific.

3.2.5. Plateaus

Plateaus cover 17,229,030 km^2 and for the most part they do not occur below the CCD. On average 0.48% of plateau area was submerged below the CCD in pre-industrial times, increasing to 0.67% at the present time. The North Pacific had the greatest areas below the pre-industrial CCD at 2.3%, which has increased to 2.4% at the present time. The Eastern Equatorial Atlantic is the only ocean region with no plateau area submerged below the CCD, either in pre-industrial times or with 300 m of hypothetical CCD shoaling. With 300 m of hypothetical CCD shoaling, the average area of plateau submerged below the CCD was predicted to increase from 0.67% at present to 1.5% (Fig. 6).

An interesting phenomenon occurs for the Nazca ridge (plateau) in the Southeast Pacific which exhibits a dramatic increase in surface area submerged by the shoaling CCD (Fig. 6). The South East Pacific contains only one major plateau feature, the Nazca Ridge (Fig. 7), covering 179,602 km^2 which presently has 1.1% of its area below the CCD but which is predicted to have 10.4% submerged with 300 m of CCD shoaling. The large increase in surface area predicted to be submerged below the CCD is explained by the geomorphology of plateaus; once the CCD rises to breach the level of the upper, flat surface of a plateau, the surface area below the CCD increases dramatically with only small amounts of CCD shoaling.

3.2.6. Guyots

Guyots cover a total area 930,370 km^2 in the 17 ocean regions dominated by the North Pacific Ocean where 43% of guyot area occurs. Harris et al. (2014) mapped 283 guyots in the world ocean having an average area of 3300 km^2; there are no guyots in the Eastern Equatorial Pacific and guyots in three ocean regions (Central Indian Ocean, Eastern Indian Ocean and the North West Atlantic) covered <10,000 km^2.

On average 23.5% of guyot area was submerged below the CCD in pre-industrial times, increasing to 24.4% at the present time. The North Pacific had the greatest areas below the pre-industrial CCD at 38.8%, which has increased to 39.7% at the present time. The Eastern

Table 5
List of EEZ's with >10% increase in area of seafloor submerged below the CCD due to hypothetical 300 m shoaling of the CCD since pre-industrial times (listed in order of increase in percent area impacted since pre-industrial times). Also listed are the EEZ area, and total percentage area that would be located below the CCD with a 300 m rise of CCD depth. The comments column lists the ocean region together with the percentage area of submarine canyons, seamounts and other features most impacted by a 300 m rise in CCD depth within each EEZ.

EEZ name (Country)	EEZ area km^2	Pre-Industrial % EEZ area below CCD	% EEZ area below CCD with 300 m rise in CCD	% Change	Comments
Bermuda (UK)	464,390	26.10	68.15	42.05	Northwest Atlantic 32.8% of terraces 25.5% Seamounts
El Salvador	95,100	0.79	37.96	37.17	Eastern Equatorial Pacific 38.4% ridge 2.9% canyons
Nauru	309,260	0.03	35.73	35.70	Western Equatorial Pacific 4.1% seamounts
Guatemala	110,660	2.22	37.46	35.24	Eastern Equatorial Pacific 74.5% ridge 2% canyons
Sri Lanka	533,550	0.84	28.95	28.11	Central Indian Ocean 34% fan, 34.9% rise, 0.4% canyons, 19.4% seamounts
Christmas Island (Aus)	327,990	3.97	31.97	28.00	Eastern Indian Ocean 15.8% seamounts
Chile - San Felix and San Ambrosio islands	450,960	10.37	38.35	27.98	Southeast Pacific 30.8% guyot 16.7% seamounts
Macquarie Island (Aus)	475,720	7.47	34.61	27.14	Southwest Pacific 14% plateau 10.8% canyons 19.6% seamounts
Cocos Islands (Aus)	467,440	6.80	29.03	22.23	Eastern Indian Ocean 15.4% escarpments 9.2% seamounts
French Polynesia	4,766,850	5.42	27.14	21.72	Central Equatorial Pacific 3.6% canyons, 15.6% seamounts
Chile	2,488,070	8.52	29.29	20.77	Southeast Pacific 50.4% rift valley, 22.8% seamounts, 19.9% slope,

Equatorial Atlantic was the only ocean region with no guyot area submerged below the CCD in pre-industrial times or at the present; a small area of 0.12% was predicted to become submerged with 200 m of CCD shoaling.

With 300 m of hypothetical CCD shoaling, the average area of guyot submerged below the CCD was predicted to increase from 24.4% at present to 30.6% (Fig. 6). A similar situation occurs for guyots as was seen for plateaus, both of which exhibit steep sides and a flat top; guyots in the Central Indian Ocean and in the North West Atlantic exhibited a dramatic increase in surface area submerged below the CCD from 10.5% and 4.2% at the present time, respectively, to 37.7% and 20.7%, respectively, with 300 m of CCD shoaling (Fig. 6).

3.2.7. Trenches

Deep ocean trenches are a unique category of geomorphic feature in that, given their extreme water depths, most of their areas are expected to be below the present CCD. Only ten ocean regions contain trenches and they are absent from the Central Equatorial Pacific, Central Indian Ocean, Eastern Equatorial Atlantic, North East Atlantic, Western Equatorial Atlantic, South East Atlantic and the Southern Indian Ocean. Trenches cover an area of 1,944,060 km^2 and on average 91.7% of trench area was submerged below the CCD in pre-industrial times, increasing to 92.4% at the present time (Fig. 6).

Since all the trench area is below the CCD in some ocean regions, there is no increase in area with shoaling of the CCD possible, and this is the pattern seen for the Northwest Atlantic, Philippine Basin, Southeast Pacific and the Southwest Pacific (Fig. 6). An interesting case occurs in the Western Indian Ocean in which the Amirante Trench (located to the west of the Seychelles) and another un-named trench located within the Carlsberg Ridge intersect the CCD, dividing the trench area of 31,894 km^2 into two halves, located above and below the CCD.

3.2.8. Spreading ridges

Spreading ridges cover an area of 6,426,930 km^2, and on average 12.3% of spreading ridge area was submerged below the CCD in pre-industrial times, increasing to 14.0% at the present time. The Philippine Basin had the greatest areas below the pre-industrial CCD at 63.1%, which has increased to 64.3% at the present time. In contrast, the North East Atlantic and Central Indian Ocean both had only 0.02% of spreading ridge area submerged below the pre-industrial CCD with virtually no change up to the present. With 300 m of hypothetical CCD shoaling, the average area of spreading ridge submerged was predicted to increase from 14.0% at present to 21.3% (Fig. 6). The Eastern Equatorial Pacific exhibited the greatest increase in spreading ridge area predicted to become submerged, increasing from 16.0% at present to 38.7% (an increase of 22.7%) with 300 m of CCD shoaling.

The highest percentages of increase in area of spreading ridges submerged below the CCD from pre-industrial times to the present (steepest slopes in Fig. 6) occurred in the Southern Indian Ocean and the South West Atlantic, regions (4.3% and 4.0%, respectively). A smaller (<0.5%) increase in surface area occurred in the Central Indian Ocean, Central Equatorial Pacific, North East Atlantic, North West Atlantic, East Equatorial Atlantic, North Pacific and Western Indian Ocean.

3.2.9. Rift valleys

Rift valleys cover an area of 674,750 km^2, and 31.8% of rift valley area on average was below the CCD in pre-industrial times, rising to 35.1% at present. The Philippine Basin had the greatest area below the pre-industrial CCD at 93.6%, which has increased to 94.4% at the present time. In contrast, the North East Atlantic and Central Indian Ocean had only 0.09% and 0.18%, respectively, of rift valley area submerged below the pre-industrial CCD increasing to 0.13% and 0.30%, respectively, at present. With 300 m of hypothetical CCD shoaling, the average area of rift valley submerged is predicted to increase from 35.1% at present to 45.2% (Fig. 6). The South East Pacific (Fig. 8) exhibits the greatest increase in rift valley area predicted to become submerged,

Table 5 (*continued*)

EEZ name (Country)	EEZ area km^2	Pre-Industrial % EEZ area below CCD	% EEZ area below CCD with 300 m rise in CCD	% Change	Comments
Réunion (Fr)	315,360	6.30	26.40	20.10	3.7% canyons, 1.9% trench Western Indian Ocean 32.2% of one guyot, 46.2% spreading ridge, 10.5% seamounts
Palmyra Atoll (US)	353,720	2.04	21.01	18.97	Central Equatorial Pacific 15.9% seamounts
Curaçaoa (Neth)	25,400	7.85	26.12	18.27	Western Equatorial Atlantic 0.2% canyons
Crozet Islands (Fr)	575,380	16.52	34.71	18.19	Southern Indian Ocean
Seychelles	1,341,480	0.67	18.64	17.97	Western Indian Ocean 0.7% canyons, 4.4% seamounts
Kiribati	1,053,240	1.33	19.19	17.86	Western Equatorial Pacific 2.0% canyons, 12.8% seamounts
Western Samoa	130,480	5.53	22.92	17.39	Western Equatorial Pacific 3.9% canyons, 14.2% seamounts
Bahamas	619,790	8.30	22.91	14.61	Northwest Atlantic 94.7% rise, 1.8% canyons, 19.6% seamounts
St. Helena (UK)	449,220	6.80	20.95	14.15	Southeast Atlantic 8.0% seamounts
Portugal	315,480	6.30	20.25	13.95	Northeast Atlantic 43.6% rise, 1.1% canyons, 2.4% seamounts
Prince Edward Islands (South Africa)	474,900	11.21	24.14	12.93	Southern Indian Ocean 18.1% rift valley, 8.7% seamounts
Aruba	29,970	7.45	19.58	12.13	Western Equatorial Atlantic 5.3% canyons
Guadeloupe	90,850	17.19	29.17	11.98	Northwest Atlantic 43% fan, 47.4% ridge, 0.5% canyons

increasing from 41.6% at present to 65.6% (an increase of 28.6%) with 300 m of CCD shoaling.

The highest percentages of increase in area of spreading ridges submerged below the CCD from pre-industrial times to the present (steepest slopes in Fig. 6) occurred in the Southern Indian Ocean and the South West Atlantic, regions (12.0% and 11.2%, respectively). A smaller (<0.5%) increase in surface area occurred in the Central Indian Ocean and in the North East Atlantic.

3.2.10. Submarine fans

Submarine fans cover an area of 7,950,110 km^2, and occurred only in 10 out of the 17 ocean regions. On average, 7.7% of fan area was below the CCD in pre-industrial times, rising to 9.8% at present. The Eastern Equatorial Pacific had the greatest percent area below the pre-industrial CCD at 36.4%, which has increased to 37.6% at the present time, but this relates only to a small area of fan that occurs in this region (24,760 km^2). Of greater significance is the area of the Bengal Fan (the largest fan complex on earth) which occurs in the Central Indian Ocean making a total fan area of 2,558,480 (32% of the world's total fan area). We find that 20% of fan area in the Central Indian Ocean was below the CCD prior to the industrial revolution, and 21% at present.

With 300 m of hypothetical CCD shoaling, the average area of fan submerged is predicted to increase from 9.8% at present to 20.3% (Fig. 6). The South East Atlantic exhibits the greatest increase in fan area predicted to become submerged, increasing from 15.9% at present to 37.1% with 300 m of CCD shoaling. The highest percentages of increase in area of submarine fan submerged below the CCD from pre-industrial times to the present (steepest slope in Fig. 6) occurred in the Western Equatorial Atlantic (increase of 9.1%).

3.2.11. Canyons

Submarine canyons cover an area of 3,794,790 km^2 and on average, 2.7% of canyon area was below the CCD in pre-industrial times, rising to 3.4% at present. Harris et al. (2014) mapped 9477 canyons in the world ocean having an average area of 460 km^2. Although submarine canyons are abundant in all ocean basins, they are mainly located on the continental slope and hence above the CCD of most ocean regions. Nevertheless, we find canyons intersect the lysocline in 12 of the 17 ocean regions (Fig. 6).

In the Philippine Basin canyons cover an area of 528,640 km^2 of which 7.6% was below the pre-industrial CCD, which is the highest percentage of canyons found below the pre-industrial CCD in any ocean region. However, canyons in the South West Atlantic (area of 283,870 km^2) have exhibited an extraordinary increase in area submerged below the CCD from 3.9% in pre-industrial times to 8.0% at the present time. Thus, at the present time it is the South West Atlantic that has the highest percentage of canyons found below the CCD in any ocean region.

With 300 m of hypothetical CCD shoaling, the average area of canyon submerged was predicted to increase from 3.4% at present to 6.5% (Fig. 6). The South West Atlantic (Fig. 9) was predicted to maintain its high rate of increase in area submerged below the CCD, rising to 17.3% of canyon area with 300 m of hypothetical CCD shoaling (Fig. 6).

3.2.12. Other categories of geomorphic features

In addition to the above, we analysed the following separate geomorphic feature categories as mapped by Harris et al. (2014): abyssal hills; abyssal mountains; bridges; hadal area; continental rise; continental slope; terrace; and trough. We found that some part of every feature category ($n = 20$) was located below the pre-industrial CCD in at least one ocean region (see Table 3).

3.3. Ocean acidification impacts in the Arctic

The intrusion of an acidified mid-depth water mass as proposed by Terhaar et al. (2020) in the 400–800 m depth range impacts upon 8 categories of seafloor geomorphic features (Table 4). The area of the

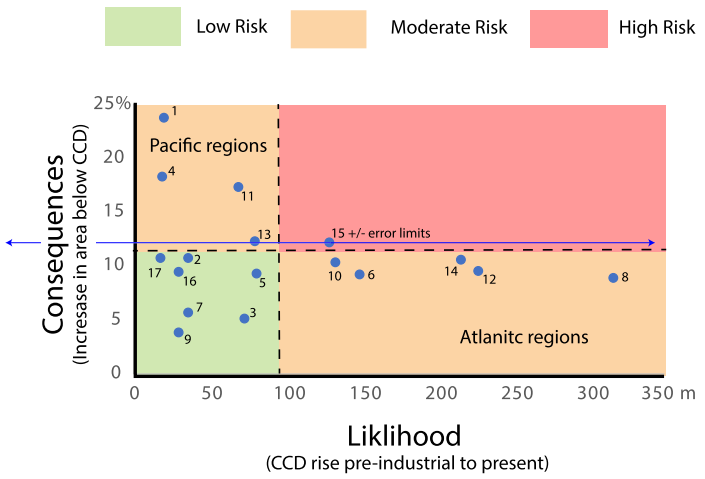

Fig. 11. Risk matrix for the 17 Ocean Regions included in this study, assuming that the change in CCD from pre-industrial times to the present is an indicator of the likelihood that the CCD will continue to rise over the next century (X-axis) and the increase in percentage of seafloor submerged below the CCD due to a hypothetical 300 m rise in the CCD is an indicator of the consequences (Y-axis). The dashed lines separate four quadrants and represent the average rise (97.8 m) of the CCD from pre-industrial times to the present and the average change in percentage of seafloor submerged below a CCD 300 m higher than present (11.0%). The western equatorial Atlantic (Ocean Region 15) is the only Ocean Region to plot in the high risk zone (error bars for Ocean Region 15 are shown to illustrate the error in estimated CCD rise for all ocean regions as per Table 1).

Arctic Ocean within the 400–800 m depth range covers 1,296,800 km^2 (Fig. 10), which was equal to about 8.3% of the Arctic basin region. The intrusion of the hypothetical acidified mid-depth water mass onto the continental shelf occurred within the deeply incised glacial troughs (Fig. 10). Apart from glacial troughs, our analysis indicates that the geomorphic features potentially most impacted by the hypothetical intrusion of an acidified mid-depth water mass are terraces, the continental slope, shelf and plateaus (Table 4). Canyons, ridges and escarpments are also potentially impacted.

3.4. Shoaling CCD impacts within Exclusive Economic Zones

The Exclusive Economic Zone (EEZ's) of some countries will be affected more by the shoaling of the CCD than others. Generally, oceanic and island nations lose more, while countries with large continental shelves lose proportionately less. Bermuda's EEZ is predicted to be the most impacted by a 300 m shoaling of the CCD above the present level, with 68% of that country's seabed becoming submerged below the CCD (Table 5). In contrast, only 6% of the US EEZ and 0.39% of the Russian EEZ were predicted to be impacted by 300 m shoaling of the CCD above the present level. Also, around 6.1% of the South China Sea EEZ (subject to multiple, overlapping claims) was predicted to be impacted by 300 m shoaling of the CCD.

In terms of geomorphic features, 14.68% of canyons in the small Caribbean island state of Antigua and Barbuda were predicted to become submerged below CCD with 300 m of shoaling, as were 33% of Bermuda's terraces and 25% of one seamount in Bermuda's EEZ. Also noteworthy was that 94% of the continental rise in the Bahama's EEZ (an area of 37,632 km^2) and 74.5% of ridge features in the Guatemalan EEZ were predicted to become submerged below CCCD with 300 m of shoaling. In the Chile EEZ, it was predicted that 50.4% of rift valley area, 19.9% of slope area and 1.9% of trench area became submerged below CCCD with 300 m of shoaling (Table 5; Supplementary Table 2).

Developing countries including El Salvador, Guatemala, Sri Lanka and Kiribati will apparently be more severely impacted by future ocean acidification than most developed countries (US, Russia and China) that are also the main sources of the greenhouse gas emissions (US EPA, 2023) that have caused ocean acidification. For example, the area of seabed projected to be submerged below the CCD within the US EEZ (lower 48 states) rose from 0.09% to 6.09% with 300 m CCD shoaling, whilst that of Russia rose from 0.04 to 0.39%.

4. Discussion

4.1. Ocean regions most at risk to future rise in CCD

To assess the risk of the seafloor area of any region being submerged below the CCD, apart from the rate at which the CCD is rising, the important factors are the amount of area that remains above the CCD and the amount of area that will be submerged with a hypothetical 300 m rising of the CCD. The pre-industrial east equatorial Atlantic was 94% above the CCD and obviously has "more to lose" than the North Pacific, two thirds of which (66%) was already below the CCD in pre-industrial times (Table 1). The average of all 17 ocean regions is 37% below the CCD in pre-industrial times.

The rise in the CCD from pre-industrial times to the present has affected some areas more than others. The Northwest Atlantic and the Southern Indian Ocean both experienced a 10% increase in area submerged below the CCD. The area below the CCD nearly doubled in the Northwest Atlantic from 13% to 23% (Table 1) and this was the region that had the largest overall rise in CCD of 316 m (Table 1). The overall global effect of the rise in the CCD since pre-industrial times is to expose an additional 12,432,100 km^2 of ocean floor (3.6% of total ocean area) below the CCD at the present time. This relatively small (average of 97.8 m) change in the depth of the CCD has therefore had a large impact on the surface area submerged below it. However, in the North Pacific, Western Indian Ocean, Philippine Basin and the East Equatorial Atlantic, there was <1% change in area from pre-industrial times to the present. <1% of the East Equatorial Atlantic is presently submerged below the CCD.

The only way to test the relative sensitivity of each ocean region to future shoaling of the CCD is to assume a uniform rise in the CCD such as has been carried out in this study. The reason is because the geomorphology of the ocean floor located at the CCD will vary between ocean regions. The surface area submerged below the rising CCD will be greatest in locations of low-gradient topography and least in areas of high-gradient topography.

For a hypothetical 300 m rising of the CCD the geographic region that will experience the greatest relative change in percentage of surface area is the Central Equatorial Pacific, where the percent area below the CCD increases from 46% in pre-industrial times to 71% (a 26% change in surface area). Heterogeneity of seafloor geomorphology located at the depth of the CCD results in differences in area submerged with a fixed amount of CCD rise. A 300 m change in CCD in the Central Equatorial Pacific results in a 26% increase in new area below the CCD, whereas the same change results in only a 4% increase in area below the CCD in the Philippine Basin.

Although this analysis does not represent any specific future

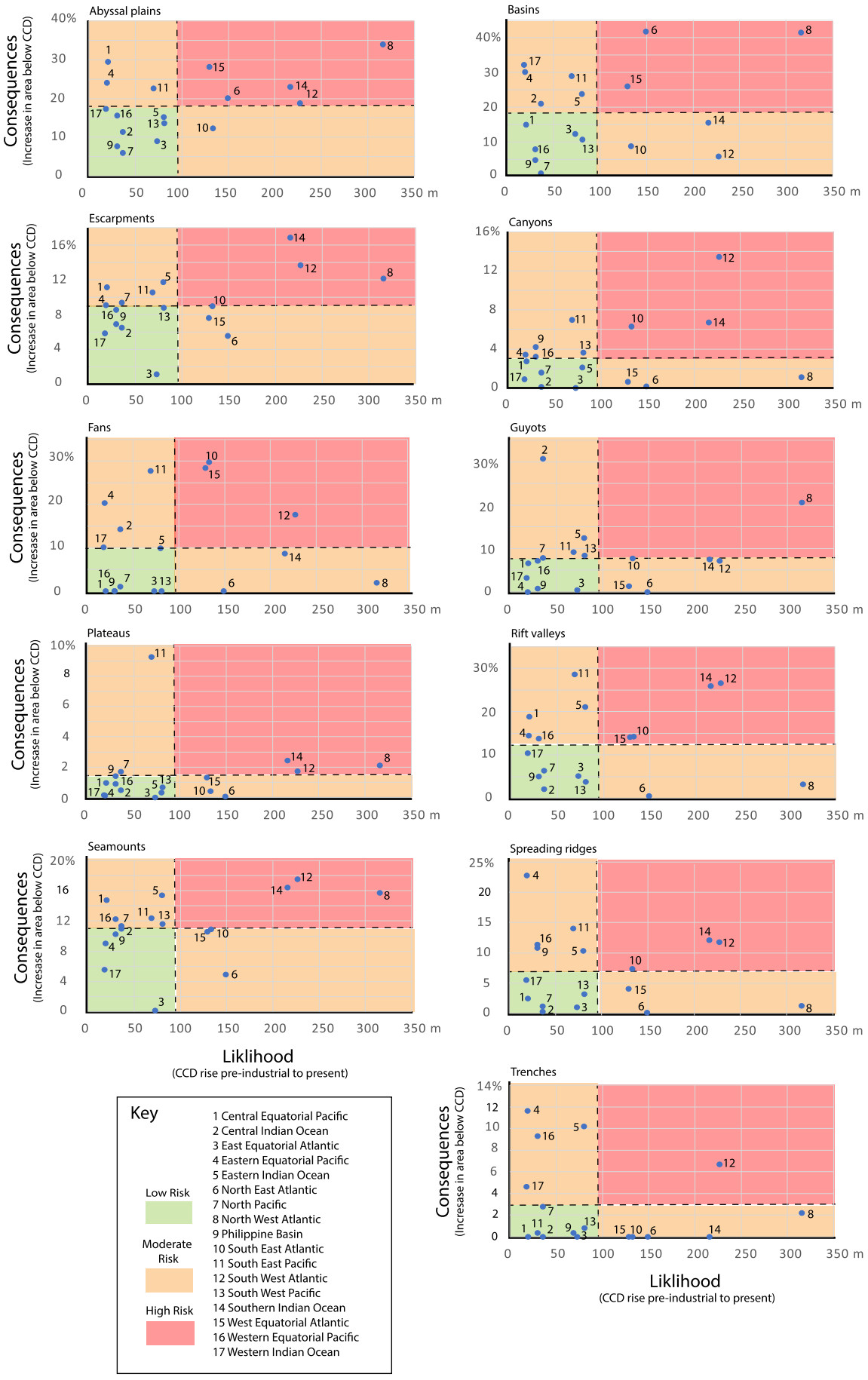

(caption on next page)

Fig. 12. Risk matrices for 11 categories of seafloor geomorphic features included in this study, as per Fig. 12. The dashed lines separate four quadrants and represent the average rise (97.8 m) of the CCD from pre-industrial times to the present and the average change in percentage of seafloor geomorphic feature submerged below a CCD 300 m higher than present (which varies between feature types). Note error bars (not shown) for CCD rise extend beyond the limits of the plotted area (see Table 1).

scenario, it does serve to illustrate how the seafloor in different ocean regions will respond to the rising CCD at some time in the future. Based on the rate at which the CCD has risen since pre-industrial times, we can predict that the NE Atlantic, which has already experienced a > 300 m rise in the CCD, might realise an additional >100 m rise in the CCD by the end of this century. In contrast, the central and eastern equatorial Pacific and western Indian Ocean regions have not experienced any significant rise in the CCD since pre-industrial times (Table 1) and so it may be some centuries before these regions will realise any significant (~100 m) rise in the CCD.

A relative risk assessment that considers the likelihood and the consequences of the CCD rising can be created using the information available. We assume that the change in CCD from pre-industrial times to the present is an indicator of the likelihood that the CCD will continue to rise at a similar pace over the next century. Next we assume that the change in percentage of seafloor submerged below the CCD due to a hypothetical 300 m rise in the CCD is an indicator of the consequences. Plotting these variables in an X-Y scatter plot provides the basis for a relative risk assessment for the 17 ocean regions included in this study (Fig. 11).

Based on this assessment we find that the area at greatest relative risk is the Western Equatorial Atlantic (Ocean Region 15; Fig. 11), which has experienced an above average rise in CCD together with an above average percentage of seafloor submerged below a CCD that is 300 m higher than present. We note that 5 of the 6 ocean regions that plot on the right-hand (high likelihood) side of Fig. 11 are in the Atlantic, along with the southern Indian Ocean (ocean region 14). Apart from ocean region 3 (Eastern Equatorial Atlantic) all of the Atlantic Ocean regions plot on the right-hand (high likelihood) side of Fig. 11.

Two groups of ocean regions at moderate risk impact from a rising CCD are: (A) those that have a high likelihood (i.e., have experienced an above average rise in CCD since pre-industrial times) but low consequences (i.e., are predicted to exhibit a below average increase in percentage of seafloor submerged below a CCD that is 300 m higher than present); and (B) low likelihood of submergence (i.e., those area that have experienced a below average rise in CCD since pre-industrial times) but high consequences (i.e., are predicted to exhibit an above average increase in percentage of seafloor submerged below a CCD that is 300 m higher than present). Group A includes the northeast Atlantic, northwest Atlantic, southeast Atlantic, southwest Atlantic and southern Indian Ocean (Ocean Regions 6, 8, 10, 12 and 14, respectively, in Fig. 11). Group B includes the central equatorial Pacific, eastern equatorial Pacific, southeast Pacific and southwest Pacific (Ocean Regions 1, 4, 11 and 13, respectively, in Fig. 11). All other Ocean Regions are in the low risk category.

4.2. Categories of geomorphic features most at risk

To assess the risk of categories of seafloor geomorphic features impacted by a rising CCD, the important factors are as for the ocean regions (i.e., the amount of area that remains above the CCD and amount of area that will be submerged with a hypothetical 300 m rising of the CCD). A result of the present study is to clearly illustrate differences between ocean regions in how the rising CCD will impact geomorphic features (Fig. 6). Each category of geomorphic feature is impacted differently among the different ocean regions. Hence the risk of any category of features becoming submerged below the rising CCD varies significantly between ocean regions. This implies that efforts to conserve biodiversity associated with different categories of geomorphic feature will need to consider each ocean region separately to define conservation priorities and targets.

For example, the percent area of submarine canyons submerged below the CCD will increase by up to 17% in the southwest Atlantic (more than any other ocean region), whereas virtually no area of submarine canyon is predicted to become submerged below a CCD that is 300 m shallower than at present in the northeast Atlantic or in the central Indian Ocean (Fig. 6). For seamounts we find that in the North Pacific over 50% of seamount area will be below a CCD that is 300 m shallower than at present, whereas virtually no area of seamount is predicted to become submerged below a CCD that is 300 m shallower than present in the eastern equatorial Atlantic (Fig. 6).

Using the same approach as for ocean regions, we have estimated the relative risk for 11 categories of geomorphic feature (Fig. 12). The likelihood (x-axis) in the risk matrices is based on the change in CCD from pre-industrial times to the present, which is the same for each category; only the consequences (y-axis) varies between categories. Abyssal plains are found to be at high risk of submergence in 5 ocean regions and rift valleys are found to be at high risk of submergence in 4 ocean regions. We find that 20 to 30% more of abyssal plains would be submerged by a 300 m rise in the CCD (note that an average of ~49% of abyssal plains are already below the CCD), located in four Atlantic Ocean regions and in the southern Indian Ocean. Seamounts and submarine canyons are at high risk in three ocean regions (Fig. 12).

Overall we see that geomorphic features in the Atlantic Ocean and southern Indian Ocean have a greater risk of being impacted by a rising CCD than those located in the Pacific Ocean and in other Indian Ocean regions. However, features in Group B of mainly Pacific Ocean regions are still at a moderate risk of impact from a rising CCD (noting the large estimated error of the CCD rise from pre-industrial times to the present; Table 1). The southeast Pacific (ocean region 11), for example, has witnessed an estimated 69 ± 308 m of CCD rise since pre-industrial times and it's geomorphic features plot in the moderate risk field for 10 out of 11 cases studied here (Fig. 12).

4.3. Impacts of acidification in the Arctic

The introduction of an acidified, mid-depth water mass around the Arctic continental margin could potentially have the greatest consequences for marine life of any ocean region. This is because ocean life in the Arctic has not previously been exposed to conditions below the CCD; and whether the Arctic benthos can adapt to life below the CCD is unknown. We can only speculate on what impact the introduction of an acidified, mid-depth water mass would have.

In their study of the benthic ecology of a Canadian glacial trough, Lacharité et al. (2020) noted the significance of a boundary at 460 m below which iceberg keel marks were absent; where the benthic fauna was dominated by molluscs and polychaetes. In their review of Arctic benthic fauna, Vedenin et al. (2021) identified a sublittoral boundary at 450–800 m that the authors suggest indicates significant changes in trophic conditions, particularly the flux of organic matter. However, the authors note that the specific environmental factors controlling organic matter flux in this depth zone are unknown and that further research is required.

Although some cold-water coral species could possibly occur in the Arctic Ocean basin, there are no published records to confirm this. One (cold water) group of coral species is adapted to a water temperature range of −1 to 3 °C but the occurrence of these species is apparently limited by geographic barriers (deep sea ridges and sills) as well as the available food supply (Buhl-Mortensen et al., 2015). It is interesting to note that cold-water coral species are commonly found at depths

between 200 and 1000 m (thus overlapping with the depth range of a hypothetical intrusion of an acidified mid-depth water mass). Further south along the Norwegian continental slope, it has been proposed by Raddatz et al. (2016) that changes in water chemistry related to glacial melting may have resulted in a hiatus in cold water coral reef growth between ~6.4 and 4.8 thousand years ago.

5. Conclusions

Based on a spatial analysis of seafloor geomorphology we have assessed the seafloor area submerged below the rising CCD caused by anthropogenic ocean acidification. We find that shoaling of the CCD since the industrial revolution has submerged 12,432,096 km^2 of ocean floor (3.6% of total ocean area) below the CCD, making a total of 40.5% of ocean floor below the CCD at present. Uniform 300 m shoaling of the CCD across all ocean regions illustrates that the surface area of seafloor submerged below the CCD rises by 14% relative to pre-industrial revolution times (total of 51% of ocean floor below the CCD). These results are significant in the context of species adaptation to climate change, since there is now evidence from at least one area of the deep ocean that the CCD is a biological barrier for some taxa (Simon-Lledó et al., 2023).

A relative risk assessment for future submergence of ocean floor below the CCD has been carried assuming that the change in CCD from pre-industrial times to the present is an indicator of likelihood and the change in percentage of seafloor submerged below the CCD due to a hypothetical 300 m rise in the CCD is an indicator of the consequences. We find that the western equatorial Atlantic is at high risk and 9 other Ocean Regions are at moderate risk. While noting the large error of the estimated CCD rise from pre-industrial times to the present, overall geomorphic features in the Atlantic Ocean and southern Indian Ocean appear to be at greater risk of impact from a rising CCD than Pacific and other Indian Ocean regions.

Out of 20 categories of geomorphic feature type, we found that some part of every feature category intersected with the lysocline and will be (or is already) submerged below the CCD in at least one ocean region. There is much regional variation between ocean regions predicted with a CCD that is 300 m shallower than present. For seamounts we find that in the North Pacific over 50% of seamount area will be below a CCD that is 300 m shallower than at present, whereas virtually no area of seamount is predicted to become submerged below in the eastern equatorial Atlantic (Fig. 6). The percent area of submarine canyons submerged below the CCD will increase by up to 17% in the southwest Atlantic (more than any other ocean region), whereas virtually no area of submarine canyon is predicted to become submerged below a CCD that is 300 m shallower than at present in the northeast Atlantic or in the central Indian Ocean (Fig. 6). Regional variation in the areas of different geomorphic feature types submerged below the CCD implies that separate conservation priorities and strategies will be needed for each ocean region to ensure their adequate representation within future marine protected area networks.

Nearly 1.3 million km^2 of the Arctic continental shelf and slope is predicted to become submerged within a mid-depth, acidified water mass proposed by Terhaar et al. (2020) by the end of the 21st century. Submarine terraces and glacial troughs incised into the continental shelf are the most impacted features. Ocean life in the Arctic has evolved in the absence of seafloor area below the CCD, and hence the formation of this acidified water mass may cause significant challenges for Arctic benthos.

Finally, we also find that the area of national Exclusive Economic Zones submerged below the rising CCD exhibits extreme variability; with 300 m of CCD shoaling we find >12% increase in area submerged below the CCD for 23 national EEZs, mainly of developing countries. The five most impacted EEZ's are Bermuda (UK), El Salvador, Nauru, Guatemala and Sri Lanka that will see >28% of their EEZ's submerged below a rising CCD. In contrast the area of seabed projected to be submerged below a CCD that is 300 m more shallow than at present rises from 0.09% to 6.09% within the US EEZ (lower 48 states), whilst that of Russia rises from 0.04 to 0.39%.

Declaration of Competing Interest

The authors declare that they have no known competing financial interests or personal relationships that could have appeared to influence the work reported in this paper.

Data availability

This study is based on the analysis of previously published spatial data as described in the methods section. Supplementary Tables 1 and 2 plus the derived GIS polygons for seafloor area located below the CCD for different ocean regions and for different geomorphic feature types are stored at www.bluehabitats.org.

Acknowledgements

The work described in this paper was produced with financial support from the Norwegian Agency for Development Cooperation (Norad), Ministry of Foreign Affairs.

References

Albright, R., Hansson, L., Cooley, S.R., Gattuso, J.-P., Marshall, P., Marshall, N., Fletcher, S., Haraldsson, G., Hoegh-Guldberg, O., 2023. Are we ready for ocean acidification? A framework for assessing and advancing policy readiness. Environ. Res. Lett. 18 (4), 041001.

Andersson, A.J., Mackenzie, F.T., 2012. Revisiting four scientific debates in ocean acidification research. Biogeosciences 9, 893–905.

Archer, D., Kheshgi, H., Maier-Reimer, E., 1998. Dynamics of fossil fuel CO2 neutralization by marine CaCO3. Glob. Biogeochem. Cycles 12, 259–276.

Becker, J.J., Sandwell, D.T., Smith, W.H.F., Braud, J., Binder, B., Depner, J., Fabre, D., Factor, J., Ingalls, S., Kim, S.H., Ladner, R., Marks, K., Nelson, S., Pharaoh, A., Trimmer, R., Von Rosenberg, J., Wallace, G., Weatherall, P., 2009. Global Bathymetry and Elevation Data at 30 Arc. Seconds Resolution: SRTM30_PLUS. Marine Geodesy. 32 (4), 355–371.

Biastoch, A., Treude, T., Rüpke, L.H., Riebesell, U., Roth, C., Burwicz, E.B., Park, W., Latif, M., Böning, C.W., Madec, G., Wallmann, K., 2011. Rising Arctic Ocean temperatures cause gas hydrate destabilization and ocean acidification. Geophys. Res. Lett. 38 (8).

Broecker, W.S., 1991. The great ocean conveyor. Oceanography 4 (2), 79–89.

Buhl-Mortensen, L., Olafsdottir, S.H., Buhl-Mortensen, P., Burgos, J.M., Ragnarsson, S.A., 2015. Distribution of nine cold-water coral species (Scleractinia and Gorgonacea) in the cold temperate North Atlantic: effects of bathymetry and hydrography. Hydrobiologia 759 (1), 39–61.

Costello, M.J., Cheung, A., De Hauwere, N., 2010. Surface area and the seabed area, volume, depth, slope, and topographic variation for the world's seas, oceans, and countries. Environ. Sci. Technol. 44 (23), 8821–8828.

El Bani Altuna, N., Rasmussen, T.L., Ezat, M.M., Vadakkepuliyambatta, S., Groeneveld, J., Greaves, M., 2021. Deglacial bottom water warming intensified Arctic methane seepage in the NW Barents Sea. Commun. Earth Environ. 2 (1), 188.

Fabry, V.J., Seibel, B.A., Feely, R.A., Orr, J.C., 2008. Impacts of ocean acidification on marine fauna and ecosystem processes. ICES J. Mar. Sci. 65 (3), 414–432.

Fischer, A., Bhakta, D., Macmillan-Lawler, M., Harris, P.T., 2019. Existing global marine protected area network is not representative or comprehensive measured against seafloor geomorphic features and benthic habitats. Ocean Coast. Manag. 167, 176–187.

Galgani, F., Michela, A., Gérigny, O., Maes, T., Tambutté, E., Harris, P.T., 2022. Marine Litter, Plastic, and Microplastics on the Seafloor. Plastics and the Ocean. A. L. Andrady. Wiley, pp. 151–197.

GRID-Arendal, 2020. Coastal and Offshore Permafrost in a Changing Arctic, Rapid Response Assessment. https://coastalrra.grida.no.

Halpern, B.S., Walbridge, S., Selkoe, K.A., Kappel, C.V., Micheli, F., D'Agrosa, C., Bruno, J.F., Casey, K.S., Ebert, C., Fox, H.E., Fujita, R., Heinemann, D., Lenihan, H.S., Madin, E.M.P., Perry, M.T., Selig, E.R., Spalding, M., Steneck, R., Watson, R., 2008. A global map of human impact on marine ecosystems. Science 319, 948–952.

Harris, P.T., 2012. Chapter 5, Surrogacy. In: Harris, P.T., Baker, E.K. (Eds.), Seafloor Geomorphology as Benthic Habitat: GeoHab Atlas of Seafloor Geomorphic Features and Benthic Habitats. Elsevier, Amsterdam, pp. 93–108.

Harris, P.T., 2020. Chapter 3 - Anthropogenic threats to benthic habitats. In: Harris, P.T., Baker, E. (Eds.), Seafloor Geomorphology as Benthic Habitat (Second Edition). Elsevier, pp. 35–61.

Harris, P.T., MacMillan-Lawler, M., 2017. Origin and characteristics of ocean basins. In: Micallef, A., Krastel, S., Savini, A. (Eds.), Submarine Geomorphology. Springer Geology. Springer, Cham, pp. 111–134.

Harris, P.T., Whiteway, T., 2009. High seas marine protected areas: benthic environmental conservation priorities from a GIS analysis of global ocean biophysical data. Ocean Coast. Manag. 52, 22–38.
Harris, P.T., MacMillan-Lawler, M., Rupp, J., Baker, E.K., 2014. Geomorphology of the oceans. Mar. Geol. 352, 4–24.
Hofmann, G.E., Barry, J.P., Edmunds, P.J., Gates, R.D., Hutchins, D.A., Klinger, T., Sewell, M.A., 2010. The effect of ocean acidification on calcifying organisms in marine ecosystems: an organism-to-ecosystem perspective. Annu. Rev. Ecol. Evol. Syst. 41 (1), 127–147.
Honisch, B., Hemming, N.G., Archer, D., Siddall, M., McManus, J.F., 2009. Atmospheric carbon dioxide concentration across the mid-Pleistocene transition. Science 324, 1,551–1,554.
Johnson, G.C., 2008. Quantifying Antarctic bottom water and North Atlantic deep water volumes. J. Geophys. Res. Oceans 113 (C5). https://doi.org/10.1029/2007JC004477.
Jutterström, S., Anderson, L.G., 2005. The saturation of calcite and aragonite in the Arctic Ocean. Mar. Chem. 94 (1), 101–110.
Kump, L., Bralower, T., Ridgwell, A., 2009. Ocean acidification in deep time. Oceanography 22 (4), 94–107.
Lacharité, M., Brown, C.J., Normandeau, A., Todd, B.J., 2020. Chapter 41 - Geomorphic features and benthos in a deep glacial trough in Atlantic Canada. In: Harris, P.T., Baker, E. (Eds.), Seafloor Geomorphology as Benthic Habitat (Second Edition). Elsevier, pp. 691–704.
Luo, Y., Boudreau, B.P., Mucci, A., 2016. Disparate acidification and calcium carbonate desaturation of deep and shallow waters of the Arctic Ocean. Nat. Commun. 7 (1), 12821.
MacMillan-Lawler, M., Harris, P.T., 2016. Multivariate Classification of Seamount Morphology: Assessing Seamount Morphotypes in Relation to Marine Jurisdictions and Bioregions. Ocean Solutions, Earth Solutions. D. J. Wright, Los Angeles, Esri. https://doi.org/10.17128/9781589484603_17d ·.
Manno, C., Sandrini, S., Tositti, L., Accornero, A., 2007. First stages of degradation of Limacina helicina shells observed above the aragonite chemical lysocline in Terra Nova Bay (Antarctica). J. Mar. Syst. 68 (1–2), 91–102.
Milliman, J.D., Troy, P.J., Balch, W.M., Adams, A.K., Li, Y.H., Mackenzie, F.T., 1999. Biologically mediated dissolution of calcium carbonate above the chemical lysocline? Deep-Sea Res. I Oceanogr. Res. Pap. 46 (10), 1653–1669.
Qi, D., Ouyang, Z., Chen, L., Wu, Y., Lei, R., Chen, B., Feely, R.A., Anderson, L.G., Zhong, W., Lin, H., Polukhin, A., Zhang, Y., Zhang, Y., Bi, H., Lin, X., Luo, Y., Zhuang, Y., He, J., Chen, J., Cai, W.-J., 2022. Climate change drives rapid decadal acidification in the Arctic Ocean from 1994 to 2020. Science 377 (6614), 1544–1550.
Raddatz, J., Liebetrau, V., Trotter, J., Rüggeberg, A., Flögel, S., Dullo, W.-C., Eisenhauer, A., Voigt, S., McCulloch, M., 2016. Environmental constraints on Holocene cold-water coral reef growth off Norway: insights from a multiproxy approach. Paleoceanography 31 (10), 1350–1367.
Sayre, R.G., Wright, D.J., Breyer, S.P., Butler, K.A., Van Graafeiland, K., Costello, M.J., Harris, P.T., Goodin, K.L., Guinotte, J.M., Basher, Z., Kavanaugh, M.T., Halpin, P.N., Monaco, M.E., Cressie, N., Aniello, P., Frye, C.E., Stephens, D., 2017. A three-dimensional mapping of the ocean based on environmental data. Oceanography 30 (1), 90–103.
Schmitz, W.J., McCartney, M.S., 1993. On the North Atlantic circulation. Rev. Geophys. 31, 29–49.
Simon-Lledó, E., Amon, D.J., Bribiesca-Contreras, G., Cuvelier, D., Durden, J.M., Ramalho, S.P., Uhlenkott, K., Arbizu, P.M., Benoist, N., Copley, J., Dahlgren, T.G., Glover, A.G., Fleming, B., Horton, T., Ju, S.-J., Mejía-Saenz, A., McQuaid, K., Pape, E., Park, C., Smith, C.R., Jones, D.O.B., 2023. Carbonate compensation depth drives abyssal biogeography in the northeast Pacific. Nat. Ecol. Evol. https://doi.org/10.1038/s41559-023-02122-9.
Sulpis, O., Boudreau, B.P., Mucci, A., Jenkins, C., Trossman, D.S., Arbic, B.K., Key, R.M., 2018. Current $CaCO_3$ dissolution at the seafloor caused by anthropogenic CO_2. Proc. Natl. Acad. Sci. 115 (46), 11700.
Sulpis, O., Agrawal, P., Wolthers, M., Munhoven, G., Walker, M., Middelburg, J.J., 2022. Aragonite dissolution protects calcite at the seafloor. Nat. Commun. 13 (1), 1104.
Sweetman, A.K., Thurber, A.R., Smith, C.R., Levin, L.A., Mora, C., Wei, C.-L., Gooday, A. J., Jones, D.O.B., Rex, M., Yasuhara, M., Ingels, J., Ruhl, H.A., Frieder, C.A., Danovaro, R., Würzberg, L., Baco, A., Grupe, B.M., Pasulka, A., Meyer, K.S., Dunlop, K.M., Henry, L.-A., Roberts, J.M., 2017. Major impacts of climate change on deep-sea benthic ecosystems. Elementa Sci. Anthropocene 5.
Terhaar, J., Kwiatkowski, L., Bopp, L., 2020. Emergent constraint on Arctic Ocean acidification in the twenty-first century. Nature 582 (7812), 379–383.
Thomas, E., 1998. Biogeography of the later Paleocene benthic foraminiferal extinction. In: Aubry, M.-P., Lucas, S.G., Berggren, W.A. (Eds.), Late Paleocene-Early Eocene Climatic and Biotic Events in the Marine and Terrestrial Records. Columbia University Press, New York, pp. 214–235.
Tozer, B., Sandwell, D.T., Smith, W.H.F., Olson, C., Beale, J.R., Wessel, P., 2019. Global bathymetry and topography at 15 arc Sec: SRTM15+. Earth Space Sci. 6 (10), 1847–1864.
United Nations, 2023a. Measure and Report Ocean Acidification - Sustainable Development Goal 14.3.1 Indicator Methodology. https://sdgs.un.org/partnerships/measure-and-report-ocean-acidification-sustainable-development-goal-1431-indicator.
United Nations, 2023b. UN delegates reach historic agreement on protecting marine biodiversity in international waters. UN News, 5 March, 2023. https://news.un.org/en/story/2023/03/1134157.
US EPA, 2023. Global Greenhouse Gas Emissions Data. accessed June, 2023,. https://www.epa.gov/ghgemissions/global-greenhouse-gas-emissions-data.
Vedenin, A., Galkin, S., Mironov, A.N., Gebruk, A., 2021. Vertical zonation of the Siberian Arctic benthos: bathymetric boundaries from coastal shoals to deep-sea Central Arctic. PeerJ 9, e11640. https://doi.org/10.7717/peerj.11640.
Widdicombe, S., Spicer, J.I., 2008. Predicting the impact of ocean acidification on benthic biodiversity: what can animal physiology tell us? J. Exp. Mar. Biol. Ecol. 366 (1), 187–197.
Woosley, R.J., 2016. Carbonate compensation depth. In: White, W.M. (Ed.), Encyclopedia of Geochemistry: A Comprehensive Reference Source on the Chemistry of the Earth. Springer International Publishing, Cham, pp. 1–2.
Zachos, J.C., Röhl, U., Schellenberg, S.A., Sluijs, A., Hodell, D.A., Kelly, D.C., Thomas, E., Nicolo, M., Raffi, M., Lourens, L.J., 2005. Rapid acidification of the ocean during the Paleocene-Eocene Thermal Maximum. Science 308, 1,611–1,615.